Quaternary Science Reviews 106 (2014) 225–246

Contents lists available at ScienceDirect

Quaternary Science Reviews

journal homepage: www.elsevier.com/locate/quascirev

A brief history of climate – the northern seas from the Last Glacial Maximum to global warming

Tor Eldevik [a, *], Bjørg Risebrobakken [b], Anne E. Bjune [b], Carin Andersson [b], H. John B. Birks [c, g, h], Trond M. Dokken [b], Helge Drange [a], Mirjam S. Glessmer [a], Camille Li [a], Jan Even Ø. Nilsen [d], Odd Helge Otterå [b], Kristin Richter [e], Øystein Skagseth [f]

[a] Geophysical Institute, University of Bergen, and Bjerknes Centre for Climate Research, Bergen, Norway
[b] Uni Research Climate, and Bjerknes Centre for Climate Research, Bergen, Norway
[c] Department of Biology, University of Bergen, and Bjerknes Centre for Climate Research, Bergen, Norway
[d] Nansen Environmental and Remote Sensing Center, and Bjerknes Centre for Climate Research, Bergen, Norway
[e] Institute for Meteorology and Geophysics, University of Innsbruck, Innsbruck, Austria
[f] Institute of Marine Research, and Bjerknes Centre for Climate Research, Bergen, Norway
[g] Environmental Change Research Centre, University College London, London, UK
[h] School of Geography and the Environment, University of Oxford, Oxford, UK

ARTICLE INFO

Article history:
Received 15 October 2013
Received in revised form
18 June 2014
Accepted 23 June 2014
Available online 6 August 2014

Keywords:
LGM-to-future
North Atlantic, Nordic seas, and Arctic
Climate
Marine
Terrestrial
Reconstruction
Observations
Climate model
Temperature
Thermohaline circulation

ABSTRACT

The understanding of climate and climate change is fundamentally concerned with two things: a well-defined and sufficiently complete climate record to be explained, for example of observed temperature, and a relevant mechanistic framework for making closed and consistent inferences concerning cause-and-effect. This is the case for understanding observed climate, as it is the case for historical climate as reconstructed from proxy data and future climate as projected by models. The present study offers a holistic description of northern maritime climate – from the Last Glacial Maximum through to the projected global warming of the 21st century – in this context. It includes the compilation of the most complete temperature record for Norway and the Norwegian Sea to date based on the synthesis of available terrestrial and marine paleoclimate reconstructions into continuous times series, and their continuation into modern and future climate with the instrumental record and a model projection. The scientific literature on a variable northern climate is reviewed against this background, and with a particular emphasis on the role of the Norwegian Atlantic Current – the Gulf Stream's extension towards the Arctic. This includes the introduction of an explicit and relatively simple diagnostic relation to quantify the change in ocean circulation consistent with reconstructed ocean temperatures. It is found that maritime climate and the strength of the Norwegian Atlantic Current are closely related throughout the record. The nature of the relation is however qualitatively different as one progresses from the past, through the present, and into the future.

1. Introduction

The poleward transport of heat and salt by the North Atlantic Ocean's thermohaline circulation (THC) is a principal component of the global climate system. Its northern surface limb – the Norwegian Atlantic Current – progressively gives up its excess heat en route toward the Arctic (Fig. 1), and thus moderates the regional climate. This interaction between a variable ocean circulation and climate is therefore central to current understanding of past, present, and projected future climate change in the northern seas region. Warm and cold phases of past regional climate back to the Last Glacial Maximum (and beyond), as well as present and future change, are understood to relate tightly with the extent and vigour of North Atlantic THC and the Norwegian Atlantic Current (e.g., Rahmstorf, 2002; Gregory et al., 2005; Rhines et al., 2008; Bakke et al., 2009; Spielhagen et al., 2011).

The term the northern seas refers collectively to the northern North Atlantic, the Nordic Seas (comprising the Norwegian, Greenland, and Iceland seas), and the Arctic Ocean, including the

* Corresponding author. Geophysical Institute, University of Bergen, PO box 7803, N-5007 Bergen, Norway. Tel.: +47 55582602.
E-mail address: tor.eldevik@gfi.uib.no (T. Eldevik).

http://dx.doi.org/10.1016/j.quascirev.2014.06.028

Norwegian Atlantic Current (NwAC) that connects the three regions (Fig. 1). The warm and saline Atlantic inflow is totally transformed as it travels the northern seas: a water-mass transformation that is the integrated signature of the NwAC's interaction with climate. Heat loss, predominantly in the Norwegian and Barents seas, and freshwater input, predominantly in the Arctic Ocean, result in two distinct outflows across the Greenland–Scotland Ridge: fresh and cold Polar Water with the East Greenland Current, and dense and cold overflow water at depth (Hansen and Østerhus, 2000; Eldevik and Nilsen, 2013).

The Atlantic Water subducts where it meets Arctic sea ice and its heat becomes essentially unavailable to the atmosphere. A shift in the marginal ice zone that separates the Atlantic and Polar domains is thus a sensitive indicator of climate change (Serreze et al., 2007; Årthun et al., 2012). The inflow has upon subduction been cooled to the extent that it is of overflow density (Mauritzen, 1996a). The overflows are however less saline and slightly colder. The subducted water, either recirculating in the vicinity of the Fram Strait or travelling the Arctic Ocean, mixes with fresher and colder water masses to finalize the transformation into overflow water (e.g., Saloranta and Haugan, 2004). The subducted branch into the Arctic proper and the regional freshwater input are the sources of the estuarine circulation that largely maintains the East Greenland Current (Stigebrandt, 1985; Eldevik and Nilsen, 2013).

An assessment of the northern THC's role in regional climate is accordingly very much about quantifying and explaining the variable temperature and strength of the Norwegian Atlantic Current. The recent Arctic-ward retreat of sea ice in the Fram Strait and Barents Sea – and the corresponding progression of the Atlantic domain (Årthun et al., 2012) – have, for example, resulted in record-warm wintertime temperatures on neighbouring Svalbard (Førland et al., 2011).

Here we review and synthesize present knowledge about climate and climate change at the THC's northern terminus. The framework of our study is presented in Section 2, and the reference records for reconstructed, observed, and projected climate are compiled and presented in Section 3. The relation between climate and predominantly northern THC – but also, for example, solar insolation – is reviewed for eight distinct climate periods or transitions in Section 4. The findings are discussed and synthesized in Section 5, which also includes a relatively simple framework that diagnoses the strength of the Norwegian Atlantic Current consistent with reconstructed Norwegian Sea temperatures. The resulting "brief history of climate" is summarized in Section 6.

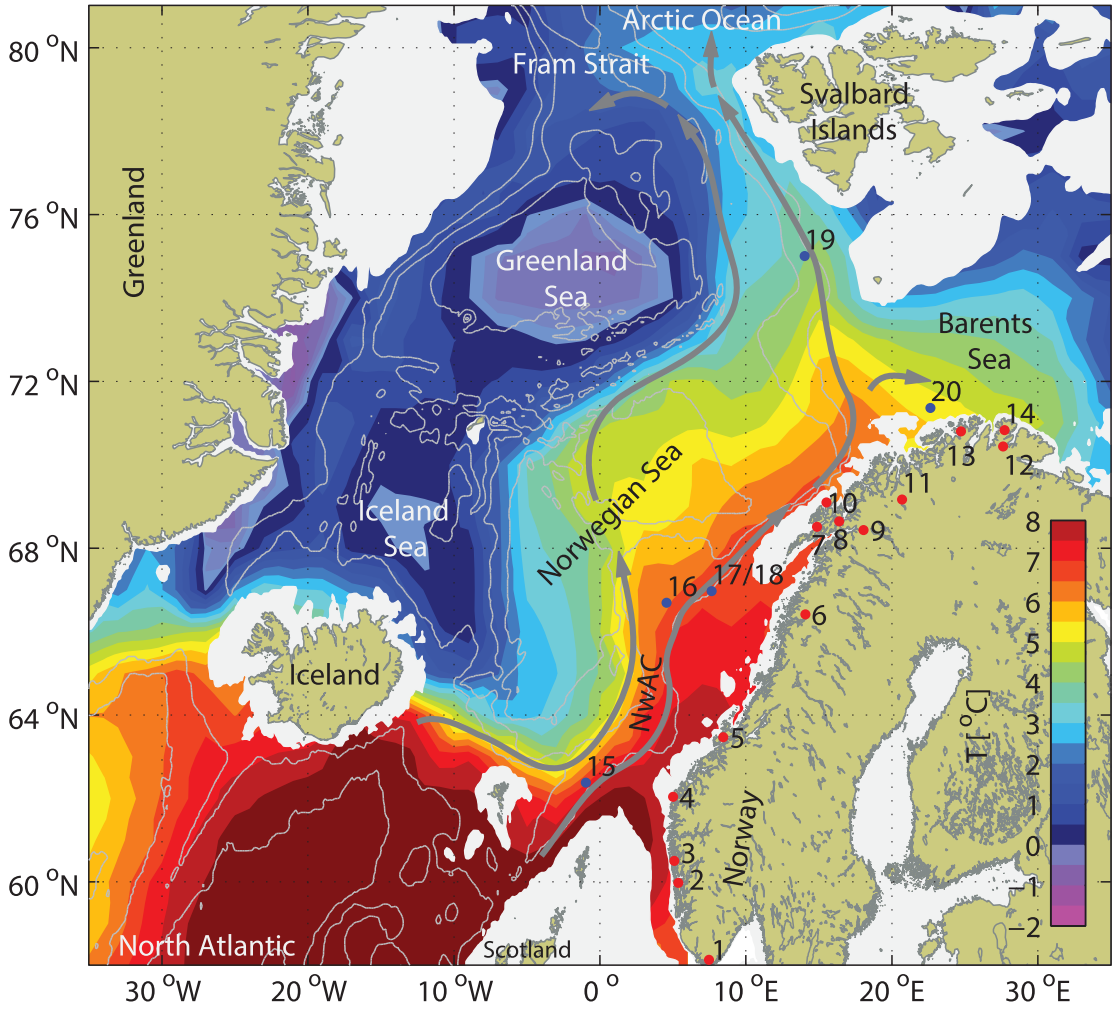

Fig. 1. Northern seas temperature climatology at 200 m depth. The arrows indicate the two branches of the Norwegian Atlantic Current (NwAC). The branches span out the region of temperate Atlantic Water that connects the North Atlantic Ocean with the Barents Sea and Arctic Ocean. Isobaths are given for every 1000 m; the figure is adapted from Eldevik et al. (2009). The numbered locations are the sites of the paleo reconstructions listed in Table 1.

2. Framework: target region, time periods, and reference climate

The specific scope of this paper is to synthesize the 'mode of operation' of northern maritime climate – in particular that relating to the Norwegian Atlantic Current – from the Last Glacial Maximum to the end of the 21st century. This will be pursued by the following rather simple, but hopefully intuitive approach. The base-line will be climate as reflected in paleoreconstructions (Figs. 2–5), in instrumental measurements (Fig. 6), and in a 21st century model projection (Fig. 7) of Norwegian and Norwegian Sea temperatures. The scientific literature on the variable northern climate is then related and chronicled with respect to this reference maritime climate, and thus a coherent description of the present understanding of the northern sea's influence on regional climate (and vice versa) is provided (Figs. 8–10).

Particular attention is given to the following eight distinct climate periods or transitions: the Last Glacial Maximum (LGM, 23.0–19.0 ka BP), Heinrich Stadial 1 (HS1, 19.0–14.6 ka BP), Bølling-Allerød (BA, 14.6–12.9 ka BP), the Younger Dryas stadial (YD, 12.9–11.7 ka BP), the early to mid Holocene (EMH, 11.7–4.0 ka BP), the late Holocene (LH, 4.0 ka BP to present), the instrumental record, and the projected climate of the 21st century. Our definition and separation of LGM and HS1 follow MARGO Project members (2009) and Barker et al. (2009), respectively. The timing used for BA and YD is in line with Rasmussen et al. (2014). Throughout the paper all references to ages of the paleorecord are presented as calendar years before present (BP), where "present" refers to AD 1950.

A premise (but also a challenge) for this synthesis is that it is possible to establish a well-defined maritime climate record – 'the thermometer', or, rather, thermometers (e.g., Fig. 2) – to which anomalous climate and ocean circulation can be related. An assessment of the northern seas' role in climate change can only be provided if there is a relatively unambiguous climate to be explained.

3. Establishment of reference temperature data sets

The data basis – the individual terrestrial and marine temperature paleoreconstructions, the related instrumental record, and a climate model projection for the 21st century – is presented in this section (Sections 3.1–3.3), including a description of how the data were aggregated into time series (Section 3.4). A most comprehensive and continuous temperature record for coastal Norway and the Atlantic domain of the northern seas, covering the LGM through to the 21st century, is accordingly compiled and the result described in Sections 3.5–3.6.

3.1. Paleoclimate

Terrestrial and marine reference datasets are compiled using previously published temperature reconstructions, supplemented by new unpublished data, from a selection of sites from coastal Norwegian lakes and from the eastern Nordic Seas (Fig. 1). The terrestrial reference dataset is established from reconstructions of past mean July surface air temperatures (SATs) based on pollen assemblages from lake sediments. Two marine reference temperature datasets are established; one based on alkenones ($U^{K'}_{37}$) and one based on planktonic foraminifer assemblages. A summary of all included sites, their geographical position, present-day temperature, and original references is given in Table 1. The selection of sites is based on the following: i) proximity to the coast and residency in the realm of the NwAC, respectively, for the terrestrial and marine sites (cf. Fig. 1); ii) time period covered by the record; iii) adequate chronological

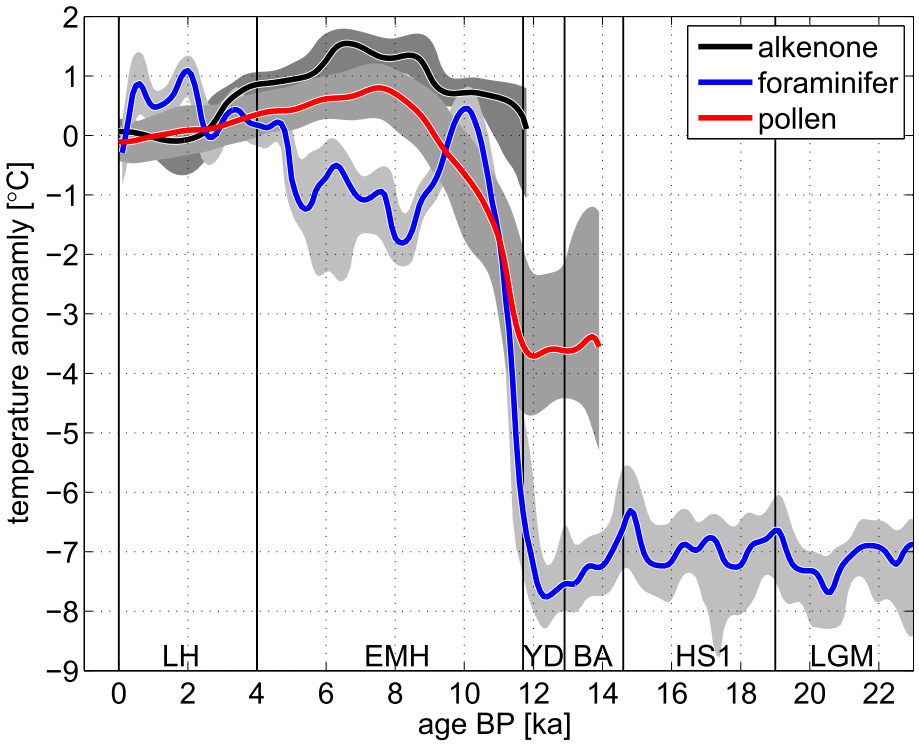

Fig. 2. The reconstructed maritime climate from the LGM through to the LH. July surface air temperature anomaly is reconstructed from pollen, and anomalous Norwegian Sea temperatures are reconstructed from alkenone and foraminifer assemblages. See Section 3 and Figs. 3 and 4 for further description of the data and methodology used, and Section 4 for a review of the different time periods and events considered.

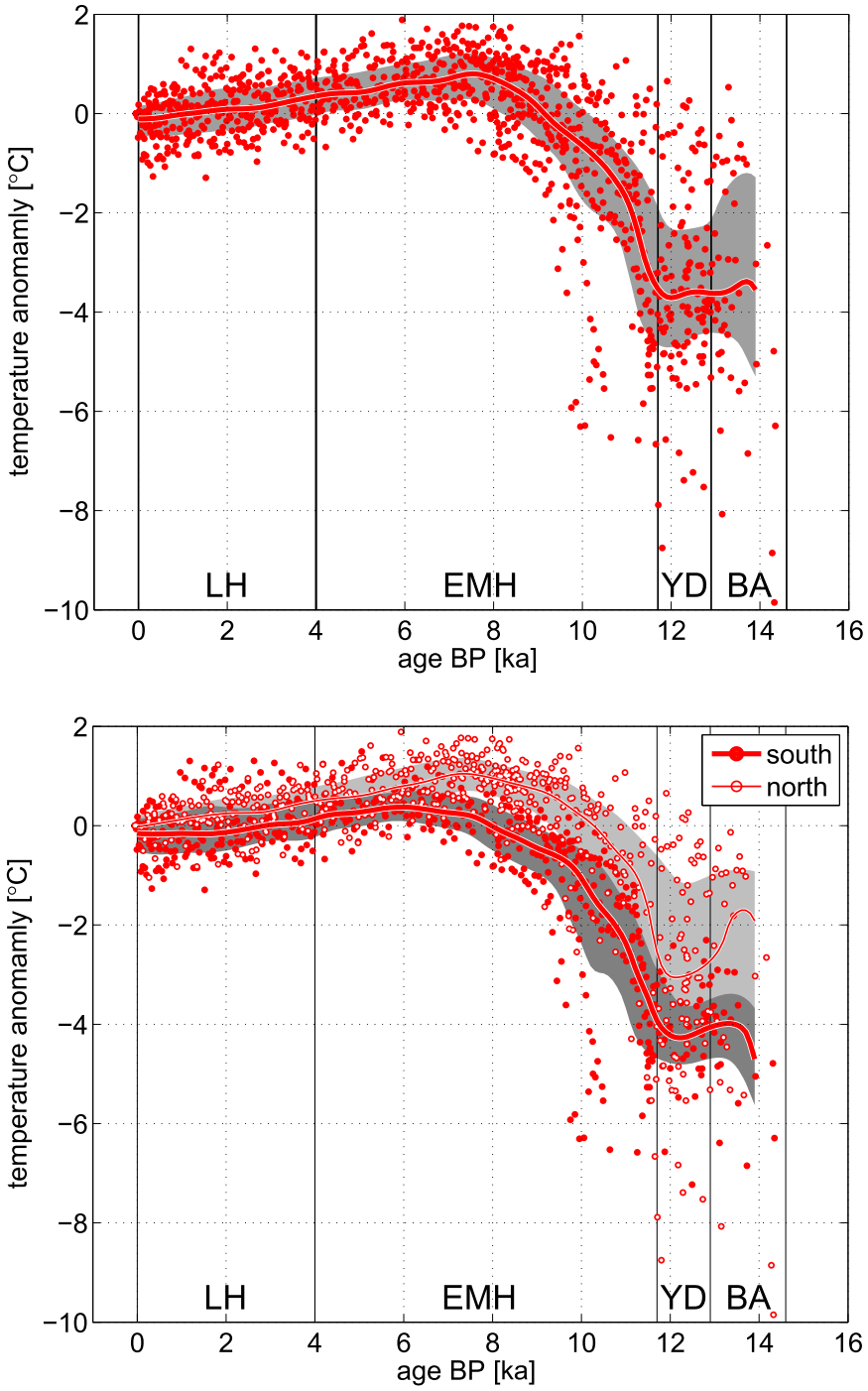

Fig. 3. Pollen-based reconstruction of July surface air temperature for coastal Norway. The scatter is the individual reconstructed anomalies, the solid line is the corresponding non-parametric regressional fit and the shading quantifies the spread. The reconstructions have been separated into southern (sites 1–5; cf. Fig. 1 and Table 1) and northern (6–14) locations in the lower panel. See Section 3 for further description of the data and methodology used, and Section 4 for a review of the different time periods and events considered.

frameworks; and iv) spatial coverage along the Norwegian coast for terrestrial sites. Adequate chronological frameworks are a premise when establishing the reference datasets. Basic information on chronologies is given below, and all the individual reconstructions are presented in Fig. 5. All age models, both for new and previously published reconstructions, are calibrated herein using the IntCal13 and Marine13 calibration curves. Detailed information concerning the age models is found in the Supplementary Tables 1 and 2 for terrestrial and marine sites, respectively.

The age-depth models developed for each of the lake cores are based on all available AMS ^{14}C ages. Calibration and age–depth modelling were done using the CLAM software (Blaauw, 2010). The calibration is based on the IntCal13 calibration curve (Reimer et al., 2013). At Jansvatnet (site 13) the age-depth model is based on linear interpolation as only a few reliable ^{14}C dates were available. Age–depth models at all the other sites were constructed using a smooth spline run through randomly sampled point estimates from calibrated dates and iterating this process a thousand times (Blaauw, 2010). Any models with age reversals were rejected.

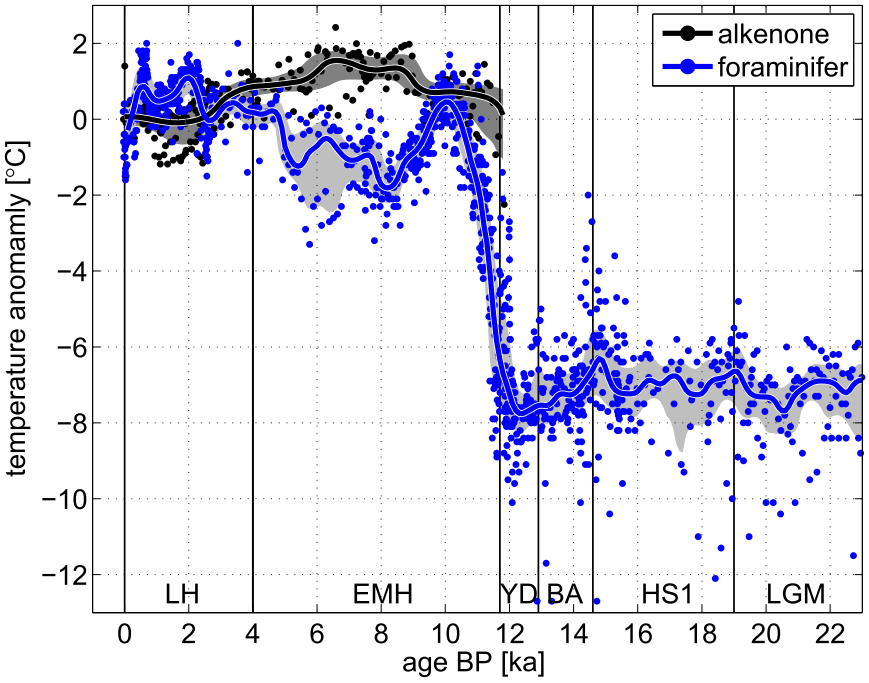

Fig. 4. Reconstructed temperature anomalies for the Norwegian Sea. The scatter is the individual reconstructed anomalies, the solid lines are the corresponding non-parametric regressional fit and the shading quantifies the spread. The reconstructions are synthesized for the two qualitatively different proxies separately (cf. Fig. 1 and Table 1). See Section 3 for further description of the data and methodology used, and Section 4 for a review of the different time periods and events considered.

Similarly, the chronologies of the marine sediment cores are based on the available AMS ^{14}C ages and, in some cores, identified ash layers (Vedde and Saksunavatn). The radiocarbon ages are calibrated using CALIB 7.0 and the Marine13 calibration dataset (Reimer et al., 2013), and corrected for the reservoir effect using $\Delta R = 7 \pm 11$ yr for MD99-2284, MD95-2010 and MD95-2011 (sites 15–17) and $\Delta R = 71 \pm 21$ yr for M23258 and PSh-5159N (sites 19 and 20) for Holocene and Bølling; $\Delta R = 250 \pm 50$ yr for YD; $\Delta R = 250 \pm 100$ yr for HS1; $\Delta R = 100 \pm 50$ yr for Allerød; and $\Delta R = 7 \pm 100$ yr for LGM. It is well known that reservoir ages may vary substantially with time. Less is known about the exact reservoir effects at given locations at given times. Holocene, YD and BA ΔR-values for the study area are taken from Bondevik et al. (2006) and Mangerud et al. (2006). There are no known ΔR values for HS1 and LGM in this region. HS1 ΔR-values were likely higher than present (e.g., Rørvik et al., 2010), and we have assumed that HS1 and YD values were comparable. The Holocene mean value is used for LGM based on the not too different oceanographic conditions in the Nordic Seas during LGM (Section 4.1). We have however increased the uncertainty used on the ΔR HS1 and LGM values to acknowledge that the absolute values are unknown. The age-depth models are established based on linear interpolation between the tie points given by the calibrated radiocarbon dates and ash layers when identified.

The marine chronologies are associated with somewhat larger uncertainty than the terrestrial chronologies, due to the need for reservoir age corrections. The calibrated age range for terrestrial dates are 40–150 years, while 70% of all marine dates have a calibrated age range <250 years. These ranges are well within the bandwidth of the reference data sets (Section 3.4). These synthesized time series are accordingly robust with respect to uncertainties related to the age models and the merging of data from different sites.

For the reconstructions of mean July SAT from the terrestrial dataset, a modern pollen-climate calibration dataset is used. This includes surface sediments from 321 lakes distributed throughout Norway and northern Sweden sampled along major gradients for both temperature and precipitation (Bjune et al., 2010). Modern mean July temperatures are estimated for each of the lakes by interpolating 1961–1990 'climate normal' data from nearby meteorological stations and adjusting for elevation, using a standard lapse rate of 0.57 °C per 100 m elevation, and for distance from coast (Seppä and Birks, 2001). Pollen-climate transfer functions based on this calibration data set are developed using weighted-averaging partial least squares (WA-PLS) regression and calibration (ter Braak and Juggins, 1993). For the sites covering the Late-Glacial and Younger Dryas time periods SAT is reconstructed using weighted averaging (WA) as this method can perform well in 'no-analogue' situations (ter Braak and Juggins, 1993). All pollen and spore percentage data are square-root transformed (Prentice, 1980) prior to WA or WA-PLS regression and calibration. For mean July temperatures the root-mean-square error of prediction is 1.13 °C and the maximum bias is 2.16 °C based on leave-one-out cross-validation (Bjune et al., 2010). The terrestrial reference temperature dataset includes all available temperature data from all the selected sites and is presented as deviations from the pollen-inferred present-day mean July temperatures at each site (Figs. 3 and 5).

Two, proxy-specific, marine reference temperature datasets are compiled to characterize the respective temperature development of the shallow summer mixed layer ($U^{K'}_{37}$ sea-surface temperature, SST) and the underlying Atlantic layer (based on foraminifer assemblages) that is directly exposed to the atmosphere in wintertime (Nilsen and Falck, 2006; Risebrobakken et al., 2011). The alkenone calibration equations and $U^{K'}_{37}$ SST values are used as originally published (Calvo et al., 2002; Marchal et al., 2002; Martrat et al., 2003; Kim and Schneider, 2004; Risebrobakken et al., 2010). Maximum likelihood regression and calibration (ter Braak and Prentice, 1988; ter Braak and van Dam, 1989) and the training-set from Kucera et al. (2005b) are used to reconstruct temperatures based on the planktonic foraminifer assemblages. For

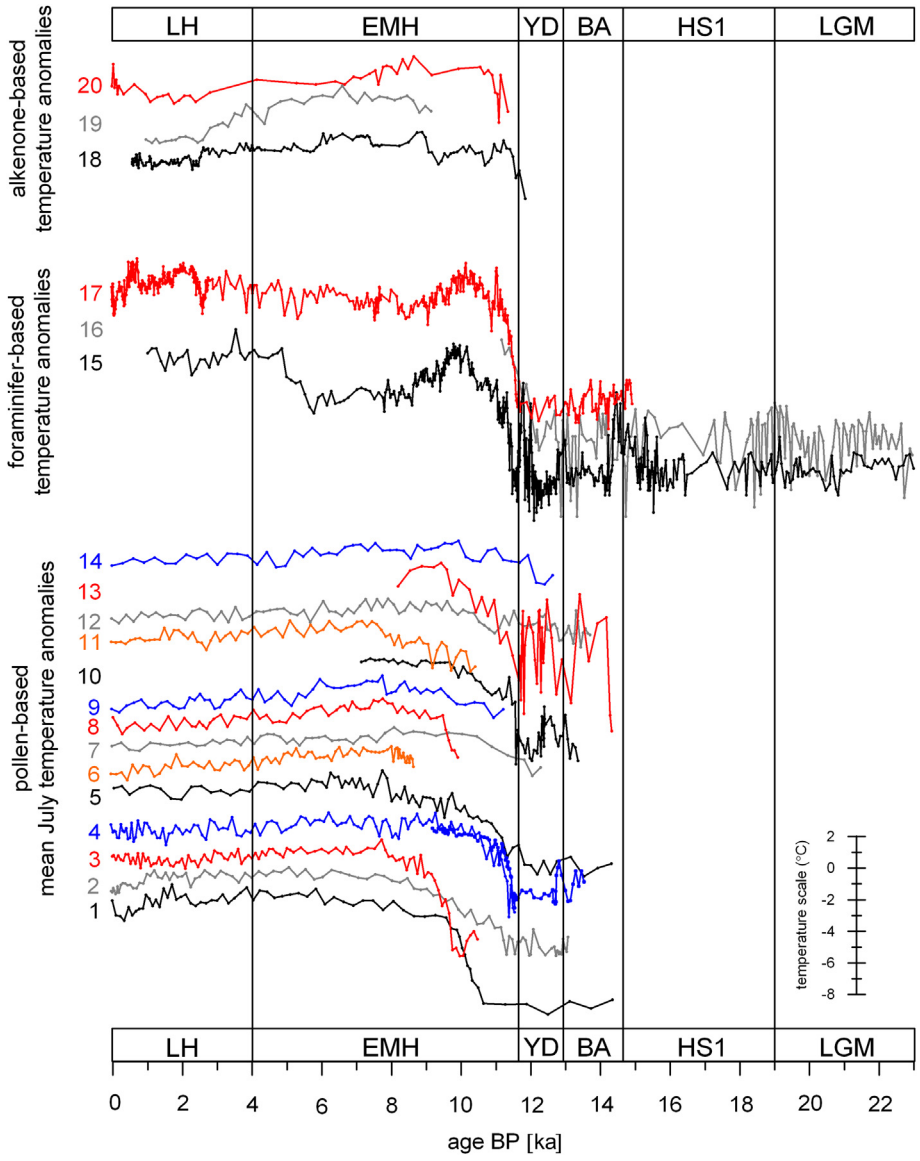

Fig. 5. All individual temperature reconstructions and age models used herein. The scale of the vertical axes is identical for all records (see inset temperature scale). The numbers refer to the site numbers of Table 1. The reader is referred to the table for further details.

both marine reference datasets all available proxy-specific temperatures are presented as deviations from the corresponding present-day temperatures for the specific proxy at the specific sites (Figs. 4 and 5). The coldest reconstructed foraminifer temperatures have the largest uncertainties. Negative anomalies thus represent a lowest estimate, and may be too cold. A detailed discussion on potential problems with absolute Holocene foraminifer temperatures for the sites used in this study can be found in Risebrobakken et al. (2011).

3.2. Observed climate

The record compiled to represent observed climate (Fig. 6) is based on established annual time series, and these series have been used as provided. The Norwegian Meteorological Institute provided annual mean Norwegian surface air temperature (SAT) based on gridded meteorological station data (e.g., Hansen-Bauer et al., 2006). Global SAT is taken from the HadCRUT4 time series (Morice et al., 2012; www.metoffice.gov.uk/hadobs/hadcrut4/). Norwegian Sea temperatures are the inflow time series of Eldevik et al. (2009) and Atlantic layer temperature from Ocean Weather Station M (OWSM, located about 100 km west of site 16; Nilsen and Falck, 2006), both extracted from the NISE dataset (Nilsen et al., 2008). In order to extend the marine record further back in time, we have included the time series of the Kola section mean temperature (Bochkov, 1982). At its downstream location in the Barents Sea, the section has been found both to reflect thermohaline changes in the Norwegian Sea upstream and hemisphere-scale climate fluctuations (Helland-Hansen and Nansen, 1909; Skagseth et al., 2008; Boitsov et al., 2012).

Estimates of Atlantic inflow/NwAC volume transport can be inferred directly from current meter measurements since the mid 1990s. A significant fraction of this variable inflow – more than 25% of variance explained for monthly data – can be inferred from observations of sea-surface height (Richter et al., 2012). Using direct historical sea-level observations from tide gauges, these authors estimated detrended volume transport anomalies for the period 1960–2006. Their resulting observation-based time series of

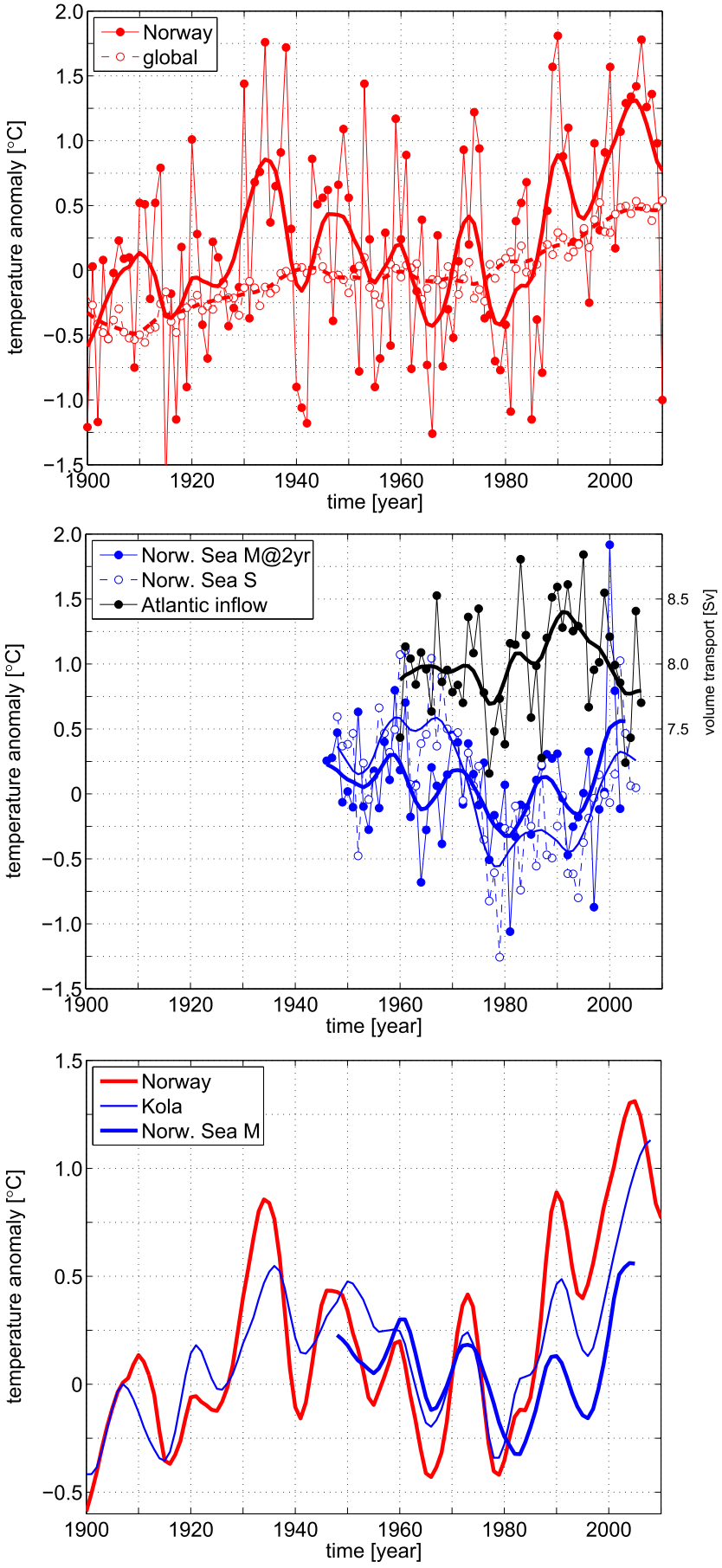

Fig. 6. The instrumental record. Panels are annual mean Norwegian surface air temperature (upper); Norwegian Sea temperatures with 'M' being Ocean Weather Station M and 'S' inflow, and Atlantic inflow volume transport (middle; 1 Sv = $10^6 m^3 s^{-1}$); and land and ocean temperature records combined, including the century-long time series from the Kola section of the Barents Sea (lower). Temperature anomalies are with respect to the 1961–1990 mean, and thick lines are 5-year low-pass filtered data.

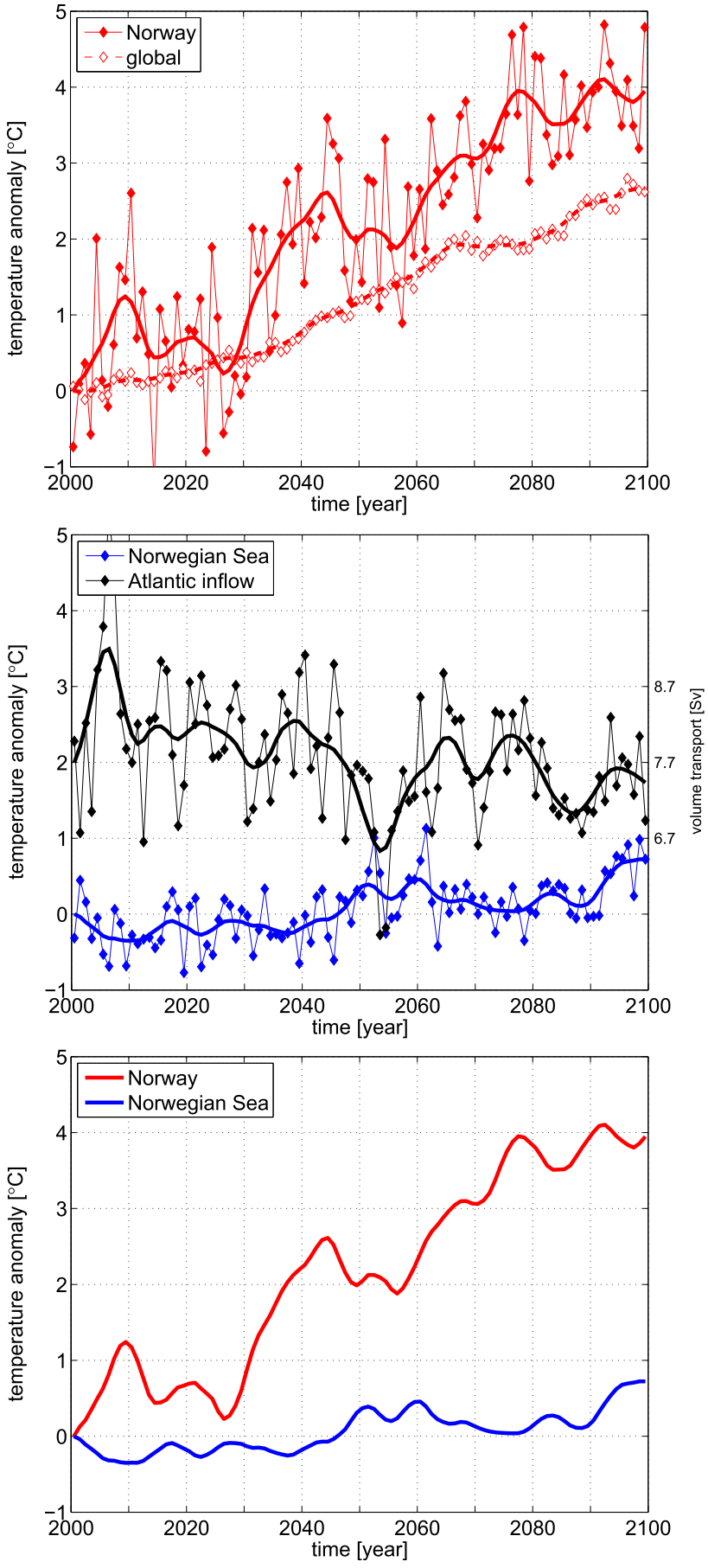
Norway
global
temperature anomaly [°C]
time [year]
Norwegian Sea
Atlantic inflow
8.7
7.7
6.7
volume transport [Sv]
Norway
Norwegian Sea

Atlantic inflow is included in the middle panel of Fig. 6 (from adding the two contributions associated with the inner and outer branch of NwAC – named "Svinøy" and "Faroe", cf. their Fig. 9 – and a representative mean value of 8 Sv, cf. Section 4.7).

3.3. Projected future climate

Future climate is described using output data from a projection with the Bergen Climate Model (BCM; Furevik et al., 2003; Otterå et al., 2009). The anthropogenic forcing of the simulation is according to the so-called A1B scenario (Johns et al., 2011), with a continuous growth in CO_2-emission through to the mid-21st century, and then a gradual but slower decrease in emissions. The resulting maritime climate is presented in Fig. 7. The Norwegian Sea temperature is in this case that of the Atlantic inflow, corresponding to "Norw. Sea S" in Fig. 6. Admittedly, what is presented is one simulation with one climate model system only. We have settled for this single example for simplicity, and because it appears representative of projected regional climate change in general (cf. Section 4.8).

3.4. Statistical methods

The paleo-data synthesized herein (cf. Table 1) constitute scatter of reconstructed data points in time and temperature. A bivariate probability density function (PDF) is calculated for each scatter, e.g., for a given proxy or coring location (Figs. 3 and 4), using the adaptive kernel density estimator of Botev et al. (2010). The kernel estimator, based on a linear diffusion process, is non-parametric including an asymptotically optimal estimate of bandwidth, i.e., the time-temperature range required to estimate the local data density. The resulting bandwidth for the applications herein is typically 400 years and 0.2 °C. The Matlab implementation referred to in Botev et al. (2010) was used as provided (Botev, 2007) for the calculations herein.

The temporal progression through the resulting bivariate PDF describes the variable temperature distribution. Synthesized climate is presented as the evolution of the three temperature quartiles in time; the second quartile – the median – is the reconstructed temperature curve, the first and third quartiles represent the spread in data (cf., e.g., Fig. 2). Note how the relatively smooth appearance of the temperature curves and spread reflect the abovementioned bandwidth.

When several reconstructed temperature records are combined, i.e., for the estimation of the variable strength of the Atlantic inflow to the Nordic Seas (Fig. 9), the following procedure is used. The PDFs – from the original paleo-data – are randomly sampled to produce a synthetic data set for the combined inference, for example the temperature difference between two coring locations. (This cannot be done directly as individual data points from each core cannot be consistently ordered into pairs for subtraction.) A PDF is then constructed from the scatter of synthetic data points as described above. The main purpose of this is to assign a data-spread to the inflow estimate consistent with the spread in the original data on which the estimate is based. The median inflow curve is for all practical purposes the same as results from using median temperature curves directly as the basis for inference.

The annual time series of the instrumental record and 21st century projections are used as provided (cf. Sections 3.2 and 3.3). When annual data are low-pass filtered, a triangular filter is used. All quantified correlations concern detrended data and are significant at the 95% confidence level unless otherwise stated, where significance (t-test) relates to the series' effective degrees of freedom (according to the integral time scale estimated from autocorrelation).

3.5. Surface air temperatures from the LGM to 2100

Lake sediment older than Bøllling-Allerød age is not found in our study region due to the extent of the Fennoscandian Ice Sheet (Gyllencreutz et al., 2007), so reconstructed atmospheric temperatures do not exist prior to 14.6 ka BP (BA; Figs. 2 and 3). SAT is inferred to be about 4 °C lower than present during the BA and YD time periods (until *ca* 12 ka BP). During these two time periods the spread in the data is large.

Colder temperatures than present are evident from the onset of sedimentation during the BA and into the EMH at *ca* 9.5 ka BP (upper panel of Fig. 3). The southern sites generally exhibit colder anomalies than the northern sites throughout the record (lower panel of Fig. 3). A rapid increase in SAT is observed in the transition period from the YD into the EMH. The warmest SAT anomaly for the entire region occurs from *ca* 9–6 ka BP, when SAT is inferred to be *ca* 1 °C higher than present-day temperatures. The warmest SAT anomaly for the southern sites occurs somewhat later (from *ca* 7.5–5 ka BP) than at the northern sites. The northern sites also show an overall higher SAT anomaly. After 6 ka BP the inferred SAT exhibits a relatively weak cooling until the present.

The instrumental record is displayed in Fig. 6 and documents a general warming trend from 1900 until 2010, about 1 °C warming both for Norwegian and global SAT. The period from 1940 to 1980 appears relatively cold. An increase in SAT is observed thereafter, until about 2005; a further and stronger temperature rise is projected through the 21st century (Fig. 7). Norwegian and global SAT increase by about 4 °C and 2.5 °C, respectively, in this particular BCM projection. Both observed and projected Norwegian SATs are characterized by decadal fluctuations with a range of about 1 °C superimposed on the generally warming trends.

3.6. Ocean temperatures from the LGM to 2100

In the marine realm, the foraminifer-based temperature reconstruction shows that cold conditions prevailed in the Norwegian Sea through the LGM, HS1, BA, and YD, with temperatures approximately 7 °C colder than present (Fig. 4). A slight warming is associated with the first part of HS1 and the transition between HS1 and BA, while the coldest temperature anomaly is seen during the YD. A strong, rapid warming characterizes the transition from YD to Holocene, from almost 8 °C colder to approximately 0.5 °C warmer temperatures than today at 10 ka BP. The 10 ka BP warming was relatively short-lived, and through most of the EMH colder than present temperatures characterized the Norwegian Sea. Through the LH, ocean temperatures are comparable to the present, but up to 1 °C warmer (Fig. 4).

Alkenone-based temperature reconstructions are only available for the Holocene part of the study interval. Similar to the pollen-based temperature reconstructions, the alkenone record documents warmer than present SSTs during EMH, with a warmest anomaly of approximately 1.5 °C between 9 and 6 ka BP, followed

Fig. 7. Projected 21st century climate. Panels are annual mean surface air temperature (upper), Norwegian Sea temperature and Atlantic inflow (middle), and land and ocean temperature time series combined (lower). Thick lines are 5-year low-pass filtered data, and anomalies are with respect to the year 2000. See Section 3.3 for a summary of the specific A1B Bergen Climate Model simulation.

Table 1
General information about the sites used for terrestrial (pollen) and marine (foraminifer and alkenone) temperature reconstructions. Time periods are Last Glacial Maximum (LGM,#1), Heinrich Stadial 1 (HS1,#2), Bølling–Allerød (BA,#3), Younger Dryas (YD,#4), Early-to-Mid Holocene (EMH,#5), and Late Holocene (LH,#6). For sites 1–14 the present-day temperatures are interpolated from nearby meteorological stations (eklima.met.no) and for sites 15–20 modern SST data are extracted from the World Ocean Atlas (http://www.nodc.noaa.gov). Detailed information on all age models is listed in Supplementary Tables 1 (terrestrial sites) and 2 (marine sites).

		Locality	Latitude	Longitude	Present-day temp., °C	Time period	No of ^{14}C dates	Reference to original data, background data and ^{14}C dates
Pollen based mean July temperatures	1	Dalane	58°15′N	8°00′E	14.9	3,4,5,6	8	Eide et al., 2006
	2	Vestre Øykjamyrtjørn	59°47′N	6°00′E	11.0	4,5,6	9	Bjune, 2005; Bjune et al., 2005
	3	Kattatjørn	60°17′N	5°06′E	13.0	5,6	6	Larsen, Peglar, Bjune & Birks[a]
	4	Kråkenes	62°02′N	5°00′E	10.5	3,4,5,6	52	Birks et al., 2000; Lohne et al., 2013; Birks & Peglar[a]
	5	Storsandvatnet	63°28′N	8°27′E	12.6	3,4,5,6	10	Birks & Peglar[a]
	6	Svanåvatnet	66°25′N	14°03′E	12.1	5,6	4	Bjune and Birks 2008
	7	Litlvatnet	68°31′N	14°52′E	12.0	4,5,6	6	Birks & Peglar[a]
	8	Myrvatnet	68°39′N	16°23′E	12.5	5,6	6	Birks & Peglar[a]
	9	Bjørnfjelltjørn	68°26′N	18°04′E	10.5	5,6	8	Bjune et al., 2010; Birks & Peglar[a]
	10	Lusvatnet	69°06′ N	15°31′E	11.0	3,4,5	23	Aarnes et al., 2012; Birks et al., 2014
	11	Dalmutladdo	69°10′N	20°43′E	11.5	5,6	11	Bjune et al., 2004
	12	Ifjord	70°26′N	27°38′E	7.6	3,4,5,6	4	Seppä, 1998; Seppä et al., 2002
	13	Jansvatnet	70°39′N	23°40′E	11.1	3,4,5	10	Birks et al., 2012
	14	Hopseidet	70°50′N	27°43′E	7.6	4,5,6	4	Seppä, 1996, 1998; Seppä et al., 2009
Foraminifer based temperatures (ML)	15	MD99-2284	62°22′N	0°58′W	11.2	1,2,3,4,5,6		Bakke et al., 2009; Dokken & Andersson[b]; Risebrobakken et al., 2011
	16	MD95-2010	66°41′N	4°33′E	10.9	1,2,3,4		Dokken & Andersson[b]
	17	MD95-2011	66°58′N	7°38′E	11.0	3,4,5,6		Andersson et al., 2003, 2010; Risebrobakken et al., 2003, 2011
Alkenone based temperatures (UK37)	18	MD95-2011	66°58′N	7°38′E	11.0	5,6		Calvo et al., 2002
	19	M23285	75°N	14°E	5.4	5,6		Marchal et al., 2002; Martrat et al., 2003; Kim and Schneider, 2004
	20	PSh-5159N	71°21′N	22°38′E	10.9	5,6		Risebrobakken et al., 2010

[a] Previously unpublished data. To be deposited in the European Pollen Database, EPD (http://www.europeanpollendatabase.net/); until then available upon request from Anne E. Bjune (anne.bjune@uni.no) or John Birks (john.birks@bio.uib.no).
[b] Previously unpublished data. To be deposited at the Data Publisher for Earth & Environmental Science, PANGAEA (www.pangaea.de); until then available upon request from Bjørg Risebrobakken (bjorg.risebrobakken@uni.no) or Trond Dokken (trond.dokken@uni.no).

by a gradual cooling (Figs. 2 and 4). Through the last 3 ka BP, the alkenone SSTs are comparable to present.

Observed Norwegian Sea temperatures are available from 1948 (Fig. 6). The record can broadly be characterized as relatively warm in the first 2–3 decades, relatively cold in the decades centred around 1980, and as warm thereafter. The recent warming does not appear exceptional in the two time series from the Norwegian Sea. However, if one considers the Kola section and the full century of data available there, a general warming through the 20th century very similar to that of the atmosphere is evident. A warming trend also extends into the projected future (Fig. 7). The NwAC is seen to warm by 0.8 °C through the 21st century, and associated with this is a 1-Sv weakening (about 12%) in volume transport. An anti-correlation between inflow volume transport and Norwegian Sea temperature is also the general case, both for observed (OWSM) and projected variability with correlations of −0.42 and −0.37, respectively, for low-pass filtered series (cf. Figs. 6 and 7; the former correlation is only significant at the 90% confidence level). We note that the range of volume transport variability roughly doubles from the observed to the projected. The latter is about 2 Sv.

4. A review of northern maritime climate

With a consistent reference climate record defined (cf. Section 3), present knowledge concerning northern maritime climate is reviewed and chronicled according to the aforementioned key periods/events: 1) the Last Glacial Maximum, 2) Heinrich stadial 1, 3) Bølling-Allerød, 4) Younger Dryas, 5) Early to Mid-Holocene, 6) Late Holocene, 7) the instrumental record, and 8) the projected warming of the 21st century. As the reviewed literature is much concerned with the quantitative concept of Atlantic Meridional Overturning Circulation (AMOC; Kuhlbrodt et al., 2007), AMOC is often referred to in this section instead of the more qualitative term THC.

4.1. Last Glacial Maximum (LGM 23.0–19.0 ka BP)

The northern seas and the North Atlantic Ocean have traditionally been considered perennially sea ice covered during the LGM (CLIMAP, 1981). More recent reconstructions, however, indicate that seasonally ice-free conditions prevailed, at least in the eastern northern seas, though variable uncertainty in reconstructed temperatures is suggested by inter-proxy differences and non-analogue thermal structure in the LGM ocean (e.g., Meland et al., 2005; Kucera et al., 2005a; de Vernal et al., 2006). Perennial sea ice was present in the Fram Strait (Müller et al., 2009). Seasonally ice-free conditions in the northern seas are also a feature of Paleo Model Intercomparison Project 2 (PMIP2) simulations, in line with the proxy-evidence (Li et al., 2010). Our reconstruction generally documents cold ocean temperatures throughout the LGM (Fig. 4), consistent with a reduced, but non-negligible poleward heat transport in the eastern part of the northern seas. Due to summer melting of surrounding ice sheets, the salinity in the central and eastern seas was lower than today, strengthening the stratification of the upper part of the water column (Meland et al., 2005; de Vernal et al., 2006). Summer melting of surrounding ice sheets has been suggested as one potential cause for the reduced salinity. Enhanced summer stratification and extended winter sea-ice cover caused subduction of the Atlantic Water at a more southern location than in the present climate (de Vernal et al., 2005).

Duplessy et al. (1988) used North Atlantic δ^{13}C values to argue that deep ocean convection during the LGM was restricted to south

of the Greenland–Scotland Ridge. This interpretation of the $\delta^{13}C$ records has since been challenged (Oppo and Lehman, 1993; Raymo et al., 2004). Newer salinity reconstructions suggest that convection took place in the northern seas (Meland et al., 2005), and bottom-water neodymium isotopic composition from the North Atlantic suggests persistent deep-water overflow from the Nordic Seas to the glacial North Atlantic throughout the LGM (Crocket et al., 2011). From the North Atlantic there is evidence for a shallower and more southern terminus of the AMOC than at present (McManus et al., 2004). Individual PMIP2 simulations of LGM climate give very different results regarding the glacial overturning circulation, ocean temperatures and sea-ice conditions in the northern seas (Otto-Bliesner et al., 2007). Assessing PMIP2 model results and reconstructions from the surface and deep Atlantic Ocean, Otto-Bliesner et al. (2007) conclude that the boundary between North Atlantic Deep Water and Antarctic Bottom Water was shallower, but that the strength of LGM overturning was probably similar to the present.

The North Atlantic Oscillation (NAO) is the leading pattern of atmospheric variability in the study region today (Hurrell, 1995). NAO-like variability exists in LGM model simulations, but exhibits some differences compared with the NAO in pre-industrial simulations, particularly in terms of seasonality and centres of action (Byrkjedal et al., 2006; Pausata et al., 2009). The models differ in this aspect, but some consistent features emerge, including the fact that the NAO-like pattern at the LGM accounts for less variability (both fraction of and actual variance explained) during LGM than today (Pausata et al., 2009).

4.2. Heinrich Stadial 1 (HS1 19.0–14.6 ka BP) – onset of termination of LGM

Heinrich Stadial 1 (HS1) covers the succession of events occurring from the end of the LGM to the onset of the Bølling-Allerød. From 19 ka BP, $^{231}Pa/^{230}Th$ and magnetic grain-size data indicate a gradual AMOC slowdown until 17.5 ka BP when a near shutdown occurred (McManus et al., 2004; Hall et al., 2006; Stanford et al., 2006). The AMOC minimum at 17.5 ka BP coincides with the onset of Heinrich Event 1 (McManus et al., 2004), characterized by a North Atlantic Ice Rafting Debris layer associated with cold SSTs and low surface salinity following massive ice-berg melting (Hemming, 2004). A sharp AMOC resumption at ~14.7 ka BP corresponds with the onset of the Bølling-Allerød (McManus et al., 2004).

Freshwater from ice-sheet melting and calving is considered a major influence through HS1, and the location of freshwater-release is important in order to affect the AMOC (Àlvarez-Solas et al., 2011). At 19 ka BP the margin of the Fennoscandian Ice Sheet (FIS) was located near the shelf break. A rapid retreat commenced before 18 ka BP, and towards the end of HS1 its margin was close to the coast (Dahlgren and Vorren, 2003). The breakdown of the FIS and Barents Sea Ice Sheet was initiated by a short-lasting warming (e.g., Lekens et al., 2006; Rørvik et al., 2010), as represented in our reconstruction around 19 ka BP, followed by cold temperatures through most of HS1 (Fig. 4). Data and models show that melting of the FIS caused an initial weakening of deep ocean convection associated with a basin-wide warming (2 °C) of the North Atlantic and the Nordic Seas at intermediate depths. The subsurface warming was important as a trigger for the inferred Laurentide Ice Shelf collapse and surge, hence the freshwater forcing of the Labrador Sea and the associated shut down of the AMOC during Heinrich Event 1 (Marcott et al., 2011; Àlvarez-Solas et al., 2011).

A direct surface-water exchange existed between the Nordic Seas and the North Atlantic during HS1 (Stanford et al., 2011). The southern Norwegian Sea foraminifer fauna was dominated by *N. pachyderma* (sin), documenting cold, polar conditions, probably with extensive winter sea ice cover and summer ocean temperatures colder than 2 °C (Rasmussen and Thomsen, 2008).

Strong depletion of the benthic $\delta^{18}O$ signal in the Nordic Seas at HS1 is a topic of ongoing discussion in terms of understanding the mechanism behind the depletion. Several theories exist, explaining the depleted benthic $\delta^{18}O$ by 1) increased temperatures (Rasmussen and Thomsen, 2008), 2) brine water formation (Dokken and Jansen, 1999; Meland et al., 2008), or 3) hyperpycnal injection of fresh meltwater (Stanford et al., 2011). Both Stanford et al. (2011) and Rasmussen and Thomsen (2008) imply cold and fresh surface water conditions in the Nordic Seas, even though they explain the depleted benthic isotope signal by different mechanisms.

4.3. Bølling-Allerød (BA 14.6–12.9 ka BP) – warm interstadial

The onset of the Bølling-Allerød (BA) is associated with an AMOC resumption at ~14.7 ka BP (McManus et al., 2004), and with a large and abrupt surface-water warming over the entire North Atlantic region (Rasmussen and Thomsen, 2008). Outflow of intermediate water from the Nordic Seas to the North Atlantic was of similar magnitude during the BA as during the Holocene, but the convected water was entrained at shallower depths than today (Meland et al., 2008). For the first time during the deglaciation, strong subsurface flow of Atlantic Water (AW) to the Arctic Ocean took place (Slubowska et al., 2005). The BA warming was, however, less pronounced in parts of the Nordic Seas than in the North Atlantic and over Greenland (e.g., Rasmussen and Thomsen, 2008). Our reconstructed temperatures show maximum warming just at the beginning of the BA, followed by a cooling through the remainder of the BA (Fig. 4). However, at deeper depths, AW entered through the Fram Strait and into the Barents Sea throughout the BA, as implied by the benthic foraminifer fauna at shallow sites (*ca* 400 m) north of Svalbard (Slubowska et al., 2005) and in the SW Barents Sea (Aagaard-Sørensen et al., 2010; Chistyakova et al., 2010). The submergence of AW nevertheless occurred farther south than today (Slubowska-Woldengen et al., 2007).

An extensive sea-ice cover characterized the BA north of Svalbard (Koç et al., 2002). In the Fram Strait, biomarkers show that ice-free conditions occurred for 200 years from 14.8 to 14.6 ka BP, followed by a variable sea ice cover until 13.2 ka BP (Müller et al., 2009). The existence of the planktonic foraminifer *N. pachyderma* (sin) implies seasonally open, but cold, water in the SW Barents Sea 13.8–12.7 ka BP (Aagaard-Sørensen et al., 2010). In the Norwegian Sea, BA surface temperature was warmer than glacial but colder than interglacial temperatures (Koç Karpuz and Jansen, 1992; Klitgaard-Kristensen et al., 2001).

Through the BA the FIS had retreated sufficiently to allow for the establishment of sparse vegetation along parts of the Norwegian coast. Our pollen-based record thus commences a little into BA and the reconstructed SAT indicates low mean July temperatures (Fig. 3).

The occurrence of an AMOC 'overshoot' at the onset of the BA is robust over different general circulation models, while evidence from proxy records is less consistent (Cheng et al., 2011). The importance of the ocean exchange between the North Atlantic and the Nordic Seas for the occurrence of an AMOC overshoot at the HS1 to BA transition, and for obtaining the full, observed magnitude of the BA warming, has been emphasized (Cheng et al., 2011). It is not clear, however, whether the overshoot is a linear response to an abrupt forcing, for example a hypothesized abrupt termination of the HS1 meltwater forcing (Liu et al., 2009), or a nonlinear AMOC response to a gradual forcing, as has been associated with AMOC in

intermediate complexity models (Knorr and Lohmann, 2007). Cheng et al. (2011) argue that the BA AMOC change was a response to a sudden exposure of subsurface ocean heat superimposed on the mean-state glacial to interglacial AMOC transition. It is not straightforward, however, to assess the role of meltwater during the deglaciation due to uncertainties in reconstructed meltwater histories, model sensitivity to freshwater forcing, as well as the importance of nonlinear feedback processes (Bethke et al., 2012).

4.4. Younger Dryas (YD 12.9–11.7 ka BP) – 'the Big Freeze'

Following the Bølling-Allerød, a rapid cooling lead to the Younger Dryas (YD) cold interval (Koç Karpuz and Jansen, 1992). Both the foraminifer-based temperature reconstruction and the SAT show that the coldest reconstructed conditions occurred during the YD (Figs. 3 and 4). The Younger Dryas was characterized by extensive cooling over Greenland, in the Nordic Seas, north of Svalbard, and in the Barents Sea (e.g., Koç Karpuz and Jansen, 1992; Alley, 2000; Klitgaard-Kristensen et al., 2001; Ebbesen and Hald, 2004; Slubowska et al., 2005; Slubowska-Woldengen et al., 2008; Bakke et al., 2009; Aagaard-Sørensen et al., 2010). One exception is north of Iceland, where there is no clear temperature change from the BA to YD (Knudsen et al., 2004). The Fennoscandian and Barents coastline was cold and dry (Seppä et al., 2002). Most of Norway was still covered by the FIS (Mangerud et al., 2011). No consensus exists on the mechanisms of the onset, stabilisation, or termination of the YD (Bakke et al., 2009; Cabedo-Sanz et al., 2012).

The anomalous cold conditions of the YD were most pronounced during winter, introducing strong seasonal contrasts (e.g., Isarin et al., 1998). The early to mid YD was characterized by a stable, extensive winter sea-ice cover in the Nordic Seas (Cabedo-Sanz et al., 2012), and strong westerlies caused cold, dry winters in central Europe (Brauer et al., 2008). The late YD was less cold and variable conditions prevailed. It is thought that increased Atlantic inflow to the Nordic Seas reduced the sea-ice extent, increased ice cover variability and affected the storm tracks more northwards (Isarin et al., 1998; Ebbesen and Hald, 2004; Bakke et al., 2009; Cabedo-Sanz et al., 2012). Increasing temperatures are inferred from the terrestrial data (Fig. 3) consistent with the development of an increased vegetation cover. The differences between the early cold and stable, and the late unstable YD phases are possibly linked to changes in seasonality, sea-ice conditions, and atmospheric forcing (Isarin et al., 1998; Denton et al., 2005; Brauer et al., 2008; Bakke et al., 2009).

The AMOC strength was reduced during the YD (McManus et al., 2004). The cause of this is uncertain, and the changes in overturning could have been both a cause and an effect of subpolar North Atlantic cooling (Brauer et al., 2008). Brine formation took place at the Nordic Seas shelves, while open ocean convection was reduced compared to the BA (Meland et al., 2008). Anomalous freshwater input has been assumed to be a cause for reduced AMOC also during YD, but consensus with respect to potential source has been lacking. Tarasov and Peltier (2005) suggested that the largest combined melt-water/iceberg discharge drained to the Arctic Ocean, using numerical models to identify this geographical release point. Murton et al. (2010) subsequently identified the flood path of the YD-drainage of Lake Agassiz to the Arctic Ocean. Wunsch (2006) proposed an alternative explanation, suggesting that the change in ocean circulation was a consequence of shifting winds.

4.5. Early to Mid-Holocene (EMH 11.7–4 ka BP) – Holocene Thermal Maximum and subsequent cooling

The transition between the YD and the Holocene is reflected by a strong and rapid temperature increase at Greenland (Rasmussen et al., 2006), over Central Europe (Blaga et al., 2013), and in all our reference time series (Fig. 2). The foraminifer-based temperature maximum at 10 ka BP (Fig. 3) is argued to reflect changes in poleward ocean heat transport, related to a reorganization of AMOC during the transition from the YD to the Holocene (Risebrobakken et al., 2011).

Warmer than present SATs and SSTs, smaller glaciers, and minimum sea-ice conditions characterize the early Holocene at high northern latitudes, and this Holocene Thermal Maximum is explained as a response to strong northern hemisphere summer insolation (e.g., Calvo et al., 2002; Nesje et al., 2005; Seppä et al., 2009; Andersson et al., 2010; Berner et al., 2011; Risebrobakken et al., 2011). The timing and magnitude of the insolation-driven Holocene thermal maximum show regional differences, probably related to the variable influence of melting ice-sheets (e.g., Kaufman et al., 2004; Blaschek and Renssen, 2012). The Holocene Thermal Maximum is followed by a cooling trend, also reflected by gradually increasing sea ice cover (Jennings et al., 2002; Rasmussen et al., 2007; Müller et al., 2012). The same long-term Holocene trend, with a Thermal Maximum followed by gradual cooling, is seen in the zonal mean 30–90°N temperature stack of Marcott et al. (2013).

The Holocene trends in both our SAT and alkenone temperature reconstruction follow the summer insolation forcing, while the trend in the foraminifer temperature reconstruction does not (Fig. 2). Different Holocene temperature trends in phytoplankton- and zooplankton-based temperature reconstructions in the Nordic Seas are noted in several studies, and probably relate to the deeper and wider zooplankton habitat, and a broader temporal zooplankton window of reproduction, relative to phytoplankton (Risebrobakken et al., 2003; Andersson et al., 2010; Leduc et al., 2010; Risebrobakken et al., 2011). There is relatively little seasonal variation in temperature below the summertime mixed layer. Hence, even though the foraminifer calcifies during summer, the implication is that the foraminifer-based reconstruction should not be dominated by seasonality. The different temperature response in surface and subsurface waters is seen in several model studies (Liu et al., 2003; Andersson et al., 2010; Risebrobakken et al., 2011; Blaschek and Renssen, 2012), and in particular in observed hydrography at OWSM (Furevik et al., 2002).

A retreating sea-ice cover, increased ocean heat transport and intensified winter storm tracks over the northern seas are identified for the mid Holocene in the Max-Planck coupled climate model (Fischer and Jungclaus, 2010). The simulated heat transport increase is caused by a strengthening of the baroclinic gyre circulation in the Nordic Seas, and to some extent by increased wind stress along the Norwegian coast. A PMIP2 mid-Holocene model intercomparison found only small changes in the NAO and mean sea level pressure compared to pre-industrial. A small NAO + like shift in mean state is indicated, if anything (Gladstone et al., 2005). A more NAO + like mid-Holocene mean state has been suggested based on, e.g., multi-proxy geochemical analysis from lake sediments sampled near Kangerlussuaq (Olsen et al., 2012), combined isotope and foraminifer fauna data from the Norwegian Sea (Risebrobakken et al., 2003), and increased winter precipitation over Scandinavia (Nesje et al., 2005).

4.6. Late Holocene (LH 4 ka BP to present) – cold period

Relative to the early-to-mid Holocene, colder SAT and SSTs, increased sea-ice cover, increased precipitation and larger glaciers are reconstructed for the late Holocene (e.g., Berner et al., 2011; Müller et al., 2012), and considered a response to the reduced northern hemisphere summer insolation. Our alkenone and SAT

reconstructions are in line with these studies as well as Marcott et al. (2013).

Several studies of marine records from the Nordic Seas suggest a late-Holocene shift towards larger amplitude and high frequency variability (e.g., Jennings et al., 2002; Risebrobakken et al., 2003; Kjennbakken et al., 2011), and major changes in sub-surface ocean temperatures are seen during the last three millennia (Andersson et al., 2003). Late-Holocene climate changes in the northern North Atlantic have been attributed to changes in the temperature and inflow of Atlantic Water to the region (e.g., Klitgaard-Kristensen et al., 2004; Eiriksson et al., 2006).

Several climate fluctuations occurred during the LH, including the cold 2.7 ka BP event, the warm Medieval Climate Anomaly (*ca* AD1000–1300), followed by the Little Ice Age (*ca* AD1400–1800), and the late 19th century warming, amplified during the late 20th/early 21st centuries (e.g., Jennings and Weiner, 1996; Andersson et al., 2003; Nesje et al., 2008; Hald et al., 2011; Cunningham et al., 2013). The relatively short duration of these climatic events prevents them from being clearly visible in our synthesized and smoothed reference records (Fig. 2). They are, however, all distinct in record 17 used in our reconstruction (Fig 5 and Table 1; Andersson et al., 2003). Proposed mechanisms for these climate variations include both internal AMOC variability and how AMOC relates to external forcing, such as total solar irradiance (Renssen et al., 2006; Latif et al., 2009; Swingedouw et al., 2011) and volcanic eruptions (Stenchikov et al., 2009; Otterå et al., 2010; Miller et al., 2012; Zanchettin et al., 2012), including related sea-ice/ocean feedbacks (e.g., Renssen et al., 2006; Miller et al., 2012). We emphasize that the briefness of this summary of mechanisms is not proportional to the rich body of literature that exists on LH climate variability; the relative briefness simply reflects that the time scales involved are short and largely unresolved in the context of the paleo time span and scales synthesized herein (e.g., Fig. 2).

4.7. The instrumental record (1900–2010) – observed climate

The regional climate is relatively well observed going back through the 20th century (Figs. 1 and 6). There is an established record of annual Norwegian SAT based on meteorological stations from 1900, and the Norwegian Sea is a well-sampled ocean due to the early explorers of modern oceanography (e.g., Helland-Hansen and Nansen, 1909), fisheries research, and decades of the 'cold war'. Overall, on multi-decadal time scales, both regional SAT and ocean temperature (represented by the Kola section for the full time-span) coincide with the global SAT – a general warming for the first three decades, followed by essentially no trend between 1940 and 1980, and subsequently, a more pronounced warming. There is additional and relatively dominant multiannual-to-decadal variability regionally; SAT variability reflects observed ocean temperatures in line with the understanding that anomalous ocean heat projects on the atmosphere (e.g., Rhines et al., 2008; Gulev et al., 2013). There is a correlation of 0.81 between 5-year low-pass filtered Norwegian SAT and OWSM (and 0.79 for SAT and the Kola section).

Estimates of Atlantic inflow volume and heat transport across the Greenland–Scotland Ridge converge at ~8 Sv and ~300 TW based on budget considerations (Worthington, 1970; Mauritzen, 1996a) and direct current measurements (Østerhus et al., 2005). The instrumental record shows clear evidence of decadal variability with a temperature range of about 1 °C (e.g., Skagseth et al., 2008; see also Fig. 6). Observed temperature (and salinity) anomalies of the northern seas, including those of the overflows, have a common source in the Atlantic inflow (e.g., Furevik, 2000; Polyakov et al., 2005; Holliday et al., 2008; Skagseth et al., 2008; Eldevik et al., 2009). The downstream propagation of anomalies is exemplified in Fig. 6 where the time series from OWSM is shifted 2 years back in time and overlaid by the inflow temperature (the lagged correlation of the two low-pass filtered time series is 0.75). Recent studies to explain the NwAC's variable strength or hydrography have accordingly identified causal factors upstream in the Atlantic proper. Marshall et al. (2001) introduced a conceptual framework showing how changes in NAO-related forcing have a direct effect on the Sverdrup circulation and accompanying hydrographic anomalies in the North Atlantic Ocean. Directly linked to the Norwegian Sea, Orvik and Skagseth (2003) found that the volume transport of NwAC was related to the North Atlantic wind-stress curl, and Hátún et al. (2005) showed that the temperature and salinity of the Atlantic inflow to the Norwegian Sea were modified by the strength and extent of the Subpolar Gyre.

There is also a direct inflow response to the NAO-forcing, from changes in the along-slope (-coast) winds acting on NwAC (Skagseth et al., 2004; Furevik and Nilsen, 2005). When integrated to annual scale based on sea level data, Richter et al. (2012) find the response is not more than ±1 Sv (cf. Fig. 6). Finally, there is evidence for an eastward shift in the extent of Atlantic Water masses in response to positive NAO forcing (Blindheim et al., 2000; Mork and Blindheim, 2000; Richter and Maus, 2011). It nevertheless remains a fact that the basic water mass distribution appears robust to observed atmospheric variability.

In short, the instrumental record (Fig. 6) is consistent with a Norwegian climate (SAT) that reflects the decadal variability of the Norwegian Sea, where thermohaline anomalies travel the Norwegian Atlantic Current, and the source of change can largely be found in the Atlantic proper. The longer-term change is aligned with observed trends in global SAT. In the instrumental record presented herein (Fig. 6), Norwegian Sea temperatures and inferred NwAC strength is generally anti-correlated (cf. Section 3.6). The result is a relatively constant NwAC heat transport consistent with the observations of Orvik and Skagseth (2005) from the Svinøy section (62°N) for the period 1995–2004.

4.8. Projected 21st century warming

Analysis of instrumental observations of surface temperature (Jones et al., 2012) and projected future global warming based on state-of-the-art coupled climate models show the most pronounced warming at high northern latitudes (Polyakov et al., 2002; Overland et al., 2011; Stroeve et al., 2012). A key factor for this polar amplification is the large fraction of land at mid and high northern latitudes, which ultimately limits the ocean's ability to absorb and store heat. Other factors, such as ice/snow and cloud albedo feedbacks, are probably also important (Serreze and Barry, 2011).

According to dynamical downscaling of CMIP5 model output over Europe for the business-as-usual scenario RCP8.5 used in IPCC AR5, large parts of Northern Scandinavia are projected to warm more than 4.5 °C by the end of the century compared to 1971–2000 (Jackob et al., 2013). More specific projections for the Svalbard region suggest an annual mean warming from 1961–90 to 2071–2100 of about 0.6 °C per decade, with even stronger warming in winter (Førland et al., 2011).

The future evolution of the Atlantic inflow to the Nordic Seas will likely be linked to projected changes in the AMOC. The climate models that participated in CMIP3 and CMIP5 simulate a typical century-scale decline in the maximum strength of the AMOC of 20–40% depending on the emission scenario (Schmittner et al., 2005; Meehl et al., 2007; Weaver et al., 2012; Cheng et al., 2013). This weakening is caused by changes in surface heat flux rather than changes in the surface freshwater flux (e.g., Gregory et al., 2005). The reduced ocean/atmosphere temperature contrast reduces the oceanic heat loss to the atmosphere. Consequently, the

poleward volume and heat transport in the models are found to decline gradually throughout this century, moderating the human-induced warming in the region.

Increased freshwater input to the northern seas is also typically associated with projected global warming, but there is little consensus concerning the sensitivity of AMOC and climate to this input, at least for the present-day warm climate (Meehl et al., 2007; Weaver et al., 2012). It should be noted that the climate models participating in CMIP3/CMIP5 do not include an active ice-sheet and therefore do not simulate the potential climate effect of enhanced melting from, e.g., the Greenland ice sheet (e.g., Weaver et al., 2012). Eldevik and Nilsen (2013) nevertheless find that the present Atlantic inflow is relatively insensitive to anomalous freshwater perturbations from combining their simple analytical model of northern seas THC with observed climatology.

The Atlantic inflow to the Nordic Seas is importantly related to North Atlantic wind forcing, and in particular to the NAO pattern as described in Section 4.7. While the future projections of NAO in CMIP2 and CMIP3 tended to show a more positive NAO in the future (e.g., Stephenson et al., 2006), a more recent study based on CMIP5 models suggests a future tendency for more negative NAO (Cattiaux et al., 2013). This would likely contribute to a reduced inflow to the Nordic Seas, in particular for the eastern inflow branch. Finally, it should be noted that multidecadal variations in Atlantic and Nordic Seas SST are expected also in a warmer world (e.g., Otterå et al., 2010; Booth et al., 2012; Cheng et al., 2013). Such variations may play a key role in shaping the forthcoming, decadal-scale climate in the northern seas.

The general picture that emerges for the future based on available model projections in the northern seas is generally in line with what is depicted from the BCM A1B simulation in Fig. 7. That is: a warming over Norway (that is stronger than the global mean, i.e., polar amplification) and a distinct, but less warming of the Norwegian Sea accompanied by a gradual reduction in AMOC (not shown) and the associated Atlantic inflow to the Nordic Seas.

5. Synthesis and discussion

Based on our reference time series (Figs. 2, 6 and 7) and the review of northern maritime climate presented in Section 4, we now proceed to synthesise the above into a coherent description of present understanding of the northern seas' influence on regional climate (and vice versa).

5.1. Northern climate change and mechanisms

The review of northern climate from the LGM to 2100 (Section 4 and references therein) points to several forcing mechanisms and feedbacks that are suggested to explain northern climate change. The explanations relate to the influence of insolation changes and changes in total solar irradiance, volcanic eruptions, atmospheric forcing, sea-ice conditions and AMOC variability. The climate responses to these depend on time scales and the background climate.

Variations in insolation forcing have a direct influence on SAT and SSTs, melting of ice sheets and sea ice, and seasonality. The reconstructions of marine and terrestrial summer climate (alkenone and pollen, respectively, in Fig. 2) are for example both interpreted to reflect largely the changes in summer solar insolation at high northern latitudes through the Holocene. The foraminifer temperatures (Figs. 2 and 4), on the other hand, cannot be directly related to insolation changes, but have been suggested to reflect changes in the strength of Atlantic inflow across the Greenland–Scotland Ridge (Risebrobakken et al., 2011) or to reflect a response to winter insolation (Moros et al., 2004).

Variation in ocean circulation is commonly invoked to explain change in the northern maritime climate. Both AMOC and the Norwegian Atlantic Current are argued to have been reduced during LGM (Section 4.1), shut down during HS1 (4.2), strong when entering the Holocene (4.5), variable through the late Holocene (4.6), and both AMOC and inflow reduction is projected for the future (4.8). These changes are for example considered to be connected to sensitivity to freshwater forcing of the deep-water formation sites (HS1, 4.2, and YD, 4.4); a sudden exposure of subsurface ocean heat (entering BA, 4.3, and Holocene, 4.5); a response to changes in external forcing like volcanic eruptions or total solar irradiance (late Holocene, 4.6); changes in North Atlantic winds (present climate, 4.7); or reduced northern air-sea heat exchange with global warming (projected climate, 4.8).

5.2. A framework for estimating the strength of the Norwegian Atlantic Current

In the following we outline an explicit and consistent framework for diagnosing changes in Atlantic inflow that can be associated with reconstructed Norwegian Sea temperatures. The strength of the Norwegian Atlantic Current can be modelled by a 'mediterranean circulation' (a so-called negative estuary, e.g., Carmack, 2007; Knudsen, 1900; Rudels, 2010; Stigebrandt, 1985),

$$UT = Q, \tag{1}$$

where U is the volume transport of the Atlantic inflow (and, by continuity, of NwAC), and T and Q, respectively, are the temperature decrease and heat loss to the atmosphere from inflow to the northern latitude where NwAC subducts beneath polar waters. Present observation-based estimates are an inflow of 8 Sv which experiences an 8 K temperature decrease upon returning as cold outflow, corresponding roughly to a 300 TW heat loss (cf. Fig. 1 and Section 4.7). The conversion between heat and temperature flux, the dimensional unit of relation (1), is that it takes 4 TW to cool 1 Sv by 1 K.

The above describes a balance between heat convergence by ocean advection and heat loss to the atmosphere. Changing heat storage within the NwAC is thus neglected in the balance. This is reasonable as the scope here is circulation change on centennial to millennia time scales. An imbalance of 10 TW, 3% of the present heat budget, corresponds to a warming of the entire Norwegian Sea, from surface to abyss, by 4 K per century. The estimate (1) is what results from Eldevik and Nilsen's (2013) more complete analytical description of northern seas THC if one assumes that the two outflows, the surface Polar Water with the East Greenland Current and the dense overflow, are of similar cold temperature. This is the case for present climate, and we are not aware of arguments to the contrary from paleo-data.

We now proceed to convert equation (1) to a form where flow strength can be inferred from reconstructed temperatures. A simplifying characteristic of observed climatology is that zonal mean NwAC temperature decreases at an approximately constant rate with increasing latitude (Fig. 8), corresponding to a relatively uniform heat loss. We therefore assume

$$Q = qL, \tag{2}$$

where q is the uniform heat loss (unit W m^{-1}), and L is the meridional extent of the Atlantic domain. The above in particular implies that if ΔT is the variable temperature decrease over the fixed latitudinal range ΔL, then

$$\frac{\Delta T}{\Delta L} = \frac{T}{L}. \tag{3}$$

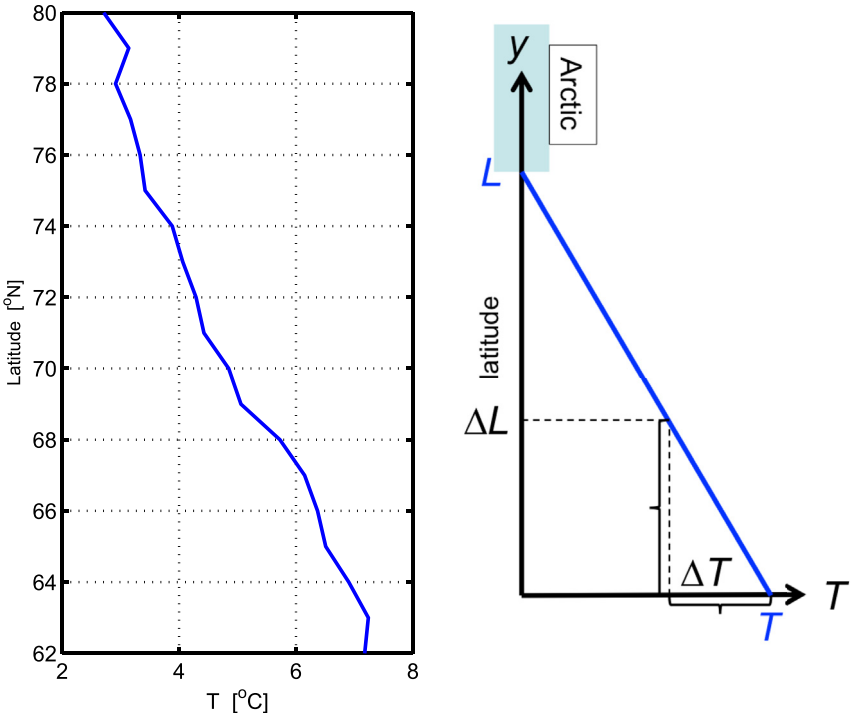

Fig. 8. Observed temperature climatology of the Norwegian Sea as a function of latitude (left panel), and the idealized linear temperature profile assumed for diagnosing paleo inflow (right panel; see Section 5.2 for further details). The climatology is concerned with Atlantic Water (salinity > 35) and taken from the NISE database (1949–2008; Nilsen et al., 2008; see also Fig. 1).

We divide the variables into mean and anomalous terms so that $T = T_0 + T'$, and so on, where subscript 0 refers to a fixed reference and prime refers to deviations from this reference state – e.g., paleo-proxy anomalies relative to present climate. The strength of Atlantic inflow can then from (1) be modelled as

$$U = \frac{q\Delta L}{\Delta T} = U_0 \frac{1 + q'/q_0}{1 + \Delta T'/\Delta T_0}; \quad U_0 = \frac{q_0 \Delta L}{\Delta T_0}. \tag{4}$$

This diagnostic relation, based on the first principle of heat conservation, describes how a *stronger* flow – from shorter residence time – corresponds to *less* temperature decrease if there is not a proportional increase in heat loss.

To avoid unrealistically large or singular flow estimates, we linearize equation (4) with respect to $\Delta T'$,

$$U = U_0 \left(1 + \frac{q'}{q_0}\right)\left(1 - \frac{\Delta T'}{\Delta T_0}\right). \tag{5}$$

This estimate is non-singular and consistent with the original relation (4) with respect to the qualitative sensitivity to changing temperatures; estimated large deviations from the reference transport are biased low (high) for negative (positive) anomalies compared to (4). The low bias is the desired "robustness" introduced by the linearization at the cost of mathematical accuracy.

The reconstructed inflow and central Norwegian Sea temperatures (site 15 and sites 16/17 combined) constitute a proxy for $\Delta T'$ (Fig. 9). The separation of sites is about $\Delta L = 5 \cdot 10^5$m, and the present temperature decrease is $\Delta T_0 = 1.5$ K (cf. Figs. 1 and 8). As seen in Fig. 1, there are also substantial zonal temperature gradients associated with the NwAC (and the sites 15–17). The NwAC and its frontal structure are however largely guided by bottom topography, particularly for the inner branch (Orvik and Niiler, 2002; Nøst and Isachsen, 2003; Skagseth et al., 2004), justifying the proxy relation. An influence of frontal excursions in reconstructed temperatures can nevertheless not be excluded (Richter and Maus, 2011; Risebrobakken et al., 2011).

A common parameterization of heat loss is to assume a linear scaling with air–sea temperature difference (e.g., Haney, 1971). In the present case, where the focus is on change rooted in the ocean (and reconstructed annual mean air temperatures are lacking), we neglect the contribution from changing SAT and assume

$$\frac{q'}{q_0} = \gamma T', \tag{6}$$

where T' is anomalous inflow temperature and γ a constant scaling factor. The resultant strength of the Norwegian Atlantic Current according to equation (1) is shown in Fig. 9, both for a uniform heat loss that is also assumed constant in time ($\gamma = 0$), and for a heat loss that accommodates weak inflow during LGM ($\gamma = 0.1$ K^{-1}). The two cases are consistent with respect to periods of increase (or decrease) in inflow, but the magnitude of change in the former is generally much more pronounced, and it levels less off going back in time from the Holocene to the LGM.

5.3. The paleo-review revisited

To first order, there seems to be a rather good agreement between the diagnosed strength of the inflow (Fig. 9) and change in inflow as discussed in the literature, the latter often based on the assumption that warmer ocean temperatures imply a stronger current (e.g., Risebrobakken et al., 2011). As reviewed in Section 4, the inflow of Atlantic Water to the Nordic Seas is argued to have been weaker than present through the LGM, HS1, BA and YD, consistent with our diagnosis. Similarly, there are arguments that a reorganization of the ocean circulation occurred during the transition between the YD and the Holocene, with a maximum advection of heat in the early EMH (Risebrobakken et al., 2011). The

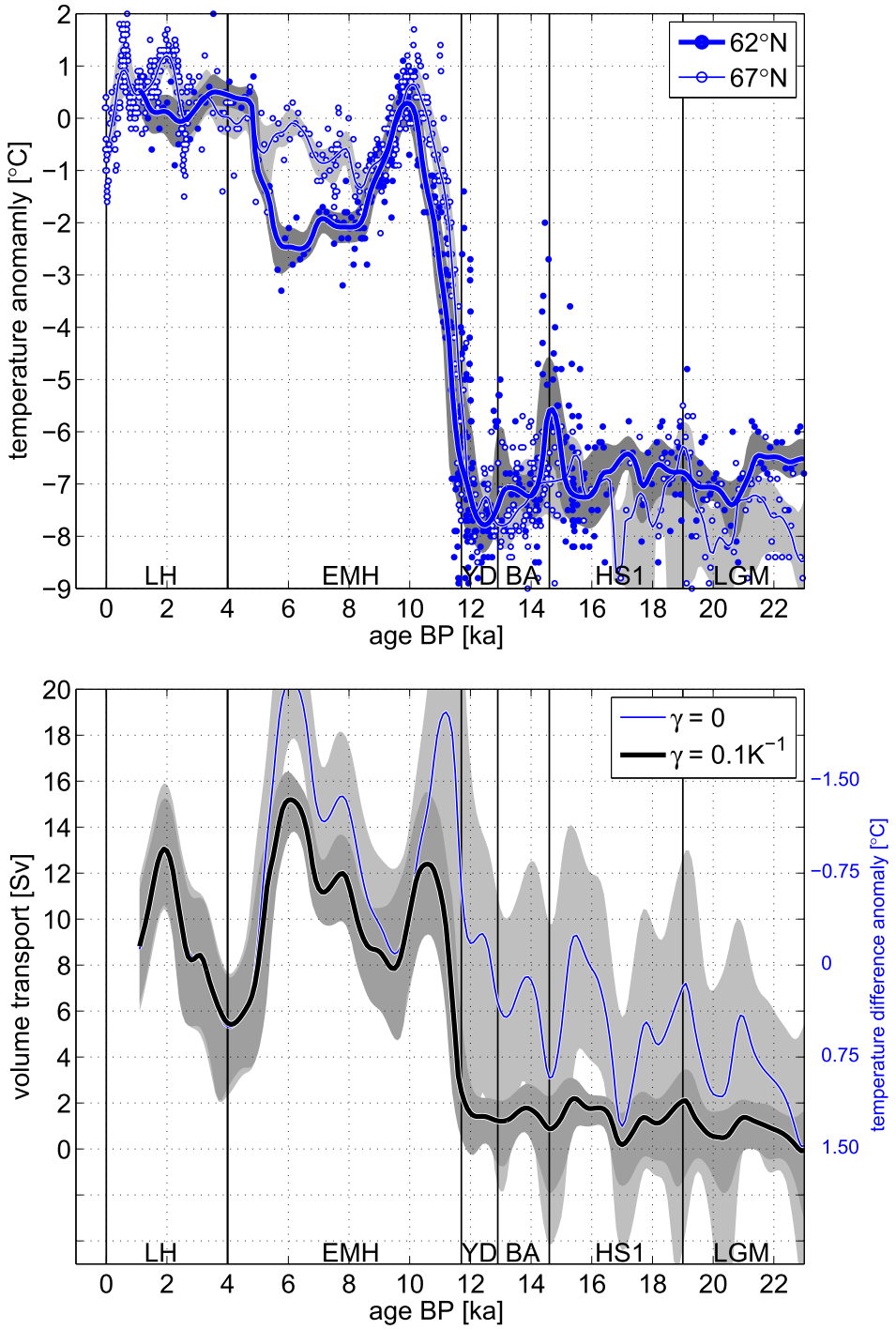

Fig. 9. Atlantic inflow inferred from reconstructed temperatures. The panels are foraminifer-based reconstructions of Norwegian Sea temperatures (sites 15 and 16/17, cf. Fig. 1 and Table 1; upper), and the consequent anomalous meridional temperature difference and proportional Atlantic inflow (thin blue curve, lower; cf. equation (5)). The thick black curve is the diagnosed inflow that also includes the contribution from a variable heat loss (per unit distance) to the atmosphere (cf. equation (6)). (For interpretation of the references to colour in this figure legend, the reader is referred to the web version of this article.)

review in Sections 4.5 and 4.6 demonstrate a consensus that the inflow of Atlantic Water has been variable through the Holocene, and that the inflow consistently has been stronger than prior to the final deglaciation, in line with our diagnosis.

If we look at the diagnosed inflow (Fig. 9) in more detail, there are inconsistencies between our estimate and implications from literature. The literature in particular suggests larger differences between LGM, HS1, BA and YD inflow strength than diagnosed, with LGM indicated to have a less weak AMOC than HS1. The LGM and HS1 are associated with a seasonal sea-ice cover and colder conditions than during BA, when AW has been traced all the way north to the Fram Strait (Section 4). A stronger inflow would therefore maybe have been expected for BA, and to some degree for LGM, compared to HS1. A stronger LGM and BA inflow than during HS1 and YD would also be in line with the Northern Hemispheric temperatures and AMOC estimates of Shakun et al. (2012).

However, no sites from the northern seas are included in their study, and the literature does imply that, e.g., the northernmost traces of AW are deeper in the water column during BA (Section 4.3).

Two other inconsistencies with previously inferred inflow relate to the timing of the EMH inflow maximum and the larger-than-present inflow diagnosed between 9 and 5 ka BP (Fig. 9). These inconsistencies can be explained by uncertainties in age control and the magnitude of reconstructed temperature anomalies at individual sites. The diagnosed peak in inflow at the transition to the Holocene is in line with arguments for maximum advection at 10 ka BP causing the general maxima in foraminifer temperatures (Section 4.5; Figs. 2 and 5). However, our maximum occurs a little earlier as the diagnosed inflow scales with the northern temperature gradient and not only temperature (equation (1)). The different timing is thus what is implied by the reconstructed temperature gradient. But given the rapid deglaciation, the estimate of the gradient is very sensitive to any uncertainties in absolute age estimates that could result in a premature reconstructed warming of the northern site prior to the southern (Fig. 9). For the period 9 to 5 ka BP, it has previously been questioned whether the reconstructed temperatures are representative of meridional temperature contrasts, a basis for our diagnosis; reconstructed anomalies implies a northern site that throughout the period is consistently – and unrealistically – warmer than the heat source, the Atlantic inflow (Risebrobakken et al., 2011).

On a more general level with respect to making inference on THC strength, there is apparently a conceptual inconsistency in the literature related to open ocean convection. The conversion and overturning of buoyant surface flow into dense water currents at depth have commonly been associated with open ocean convection (Nansen, 1906; Marshall and Schott, 1999; Rahmstorf, 2002). Convection, for example in the Greenland Sea, is therefore generally described and assessed as a critically limiting factor for THC, including NwAC (e.g., Aagaard et al., 1985; Hansen et al., 2001). The concept has been invoked to understand a changing AMOC in general, including possible future climate change, and variability and abrupt change between and within reconstructed paleo climates (e.g., Rahmstorf, 2002; Bryden et al., 2005; Dong and Sutton, 2005).

The above paradigm, originally rooted in the instrumental record, nevertheless appears at odds with the present oceanographic literature. It is now known that the process of open ocean convection *per se* cannot be associated with large-scale net sinking of

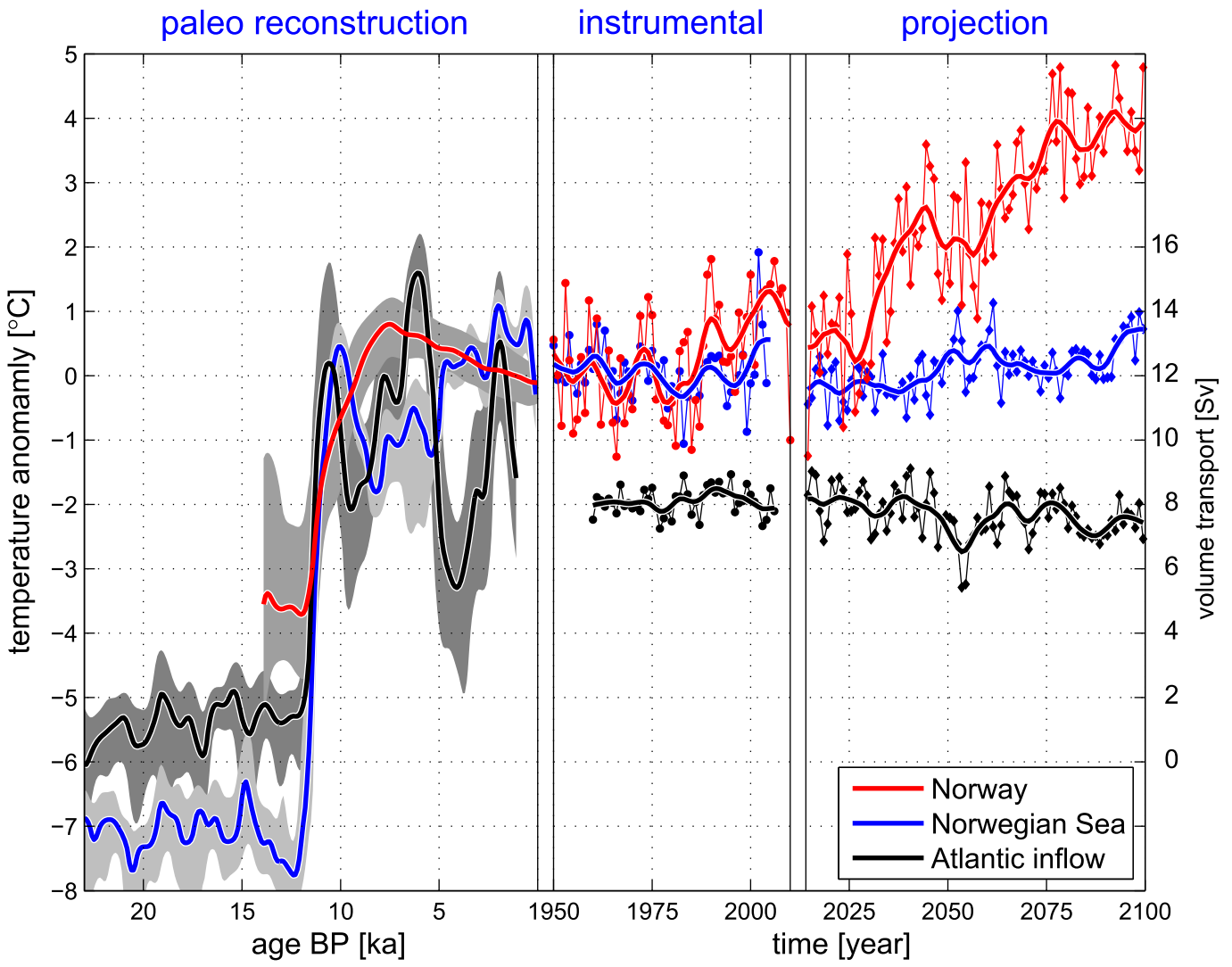

Fig. 10. Northern maritime climate from the LGM to the end of the 21st century. Time series are land (red) and ocean (blue) temperatures, and the strength of Atlantic inflow (black) as reconstructed, observed, and projected. Note that the time scale is compressed by a factor 1:200 for reconstructed climate. The figure is a composite of Figs. 2, 6, 7 and 9; please refer to these for further details. (For interpretation of the references to colour in this figure legend, the reader is referred to the web version of this article.)

water masses (e.g., Spall and Pickart, 2001; Straneo, 2006). It has in particular been observed that a previously inferred causality (Hansen et al., 2001) between northern deep ventilation and dense overflow from the Nordic Seas does not hold (Olsen et al., 2008). Furthermore, water-mass transformation and ocean heat loss are predominantly associated with the gradual cooling of boundary currents, i.e., with NwAC for the case of the Nordic Seas (e.g., Mauritzen, 1996b; Isachsen et al., 2007). The distinct downstream cooling through the Norwegian Sea is the observational manifestation of this process (cf. Figs. 1 and 8; the left hand side of the diagnostic relation, equation (1), is a quantification of this cooling). We emphasize that the above does not imply convection to be unrelated to THC; in the absence of Atlantic inflow, there can be no deep (thermal) convection in the Greenland Sea.

5.4. The northern seas from Last Glacial Maximum to global warming

Land and ocean temperature records have been compiled and presented for past, present, and future climate (Figs. 2, 6 and 7). There are corresponding observation- and model-based time series of Atlantic inflow volume transports in the latter two cases. An inflow quantitatively consistent with reconstructed ocean temperatures is diagnosed as described in Section 5.2 (Fig. 9; the case $\gamma = 0.1\ K^{-1}$ is included in the following). The resulting composite of northern maritime climate is presented in Fig. 10. We believe this description to be rather unique, both with respect to the relative completeness of the paleo record, and to the unified documentation of past, present, and future climate variability. Note however that whereas the transient structures of present and future are directly comparable, this does not apply for their comparison with the past. The temporal range of the former two records is shorter than the temporal resolution of the synthesized reconstruction. This caveat is fundamental, but not specific to the present assessment; it is generic to the interpretation of observed climate on the background of the reconstructed past (and vice versa).

6. A brief history of climate

An ocean-based summary of our review and consequent synthesis is visualized in Fig. 10 (notwithstanding the caveats with respect to, e.g., proxy interpretation, Sections 5.2 and 5.3, and the different time scales considered, Section 5.4). The strength of the Atlantic inflow – and by continuity that of the Norwegian Atlantic Current – may explain reconstructed temperatures when diagnosed according to the conservation of heat. The inflow is estimated to be relatively marginal during the cold millennia, and then to shift to a mean level like the present to accommodate Holocene conditions in the northern seas region (Sections 5.2 and 5.3). The projected future is qualitatively different. Under global warming, the inflow is weakening to accommodate less poleward heat transport and, consistently, less temperature contrast between the warming ocean and atmosphere (Section 4.8). The instrumental record is again different; the atmosphere in general reflects anomalous ocean temperatures provided by an anti-correlated inflow suggesting a relatively constant poleward heat transport (Section 4.7). One may however speculate that the (slightly) weaker inflow with recent ocean and land warming (from about 1990, cf. Fig. 10) is evidence of a present climate that is becoming qualitatively like the projected climate.

Acknowledgements

This research was supported by the Research Council of Norway (RCN) through the funding of the Bjerknes Centre as a national "Centre of Excellence" (2003–2012). Previously unpublished data are from the RCN-funded projects KILO, NORPAST, NORPEC, and Setesdal, and the EU FP7-funded project Past4Future. Support was also provided by the Centre for Climate Dynamics at the Bjerknes Centre. The NISE data were provided by the Marine Research Institute, Iceland; Institute of Marine Research, Norway; the Faroese Fisheries Laboratory; and the Geophysical Institute, University of Bergen, Norway. The authors thank two anonymous reviewers and the guest editor Sune O. Rasmussen for their specific and constructive suggestions that improved the manuscript.

Appendix A. Supplementary data

Supplementary data related to this article can be found at http://dx.doi.org/10.1016/j.quascirev.2014.06.028.

References

Aagaard, K., Swift, J.H., Carmack, E.C., 1985. Thermohaline circulation in the arctic mediterranean seas. J. Geophys. Res. 90, 4833–4846.
Aagaard-Sørensen, S., Husum, K., Hald, M., Knies, J., 2010. Paleoceanographic development in the SW barents sea during the late Weichselian-early holocene transition. Quat. Sci. Rev. 29, 3442–3456.
Aarnes, I., Bjune, A.E., Birks, H.H., Balascio, N.L., Bakke, J., Blaauw, M., 2012. Vegetation response to rapid climatic change during the last deglaciation 13,500-8,000 years ago on southwest Andøya, arctic Norway. Veget Hist. Archaeobot. 21, 17–35.
Alley, R.B., 2000. The Younger Dryas cold interval as viewed from central Greenland. Quat. Sci. Rev. 19, 213–226.
Àlvarez-Solas, J., Montoya, M., Ritz, C., Ramstein, G., Charbit, S., Dumas, C., Nisancioglu, K., Dokken, T., Ganopolski, A., 2011. Heinrich event 1: an example of dynamical ice-sheet reaction to oceanic changes. Clim. Past 7, 1297–1306.
Andersson, C., Pausata, F., Jansen, E., Risebrobakken, B., Telford, R., 2010. Holocene trends in the foraminiferal record from the Norwegian Sea and the North Atlantic. Clim. Past 6, 179–193.
Andersson, C., Risebrobakken, B., Jansen, E., Dahl, S.O., 2003. Late Holocene surface-ocean conditions of the Norwegian Sea (Vøring Plateau). Paleoceanography 18, 1044. http://dx.doi.org/10.1029/2001PA000654.
Årthun, M., Eldevik, T., Smedsrud, L.H., Skagseth, Ø., Ingvaldsen, R., 2012. Quantifying the influence of Atlantic heat on barents sea ice variability and retreat. J. Clim. 25, 4736–4743.
Barker, S., Diz, P., Vautravers, M.J., Pike, J., Knorr, G., Hall, I.R., Broecker, W.S., 2009. Interhemispheric Atlantic seesaw response during the last deglaciation. Nature 457, 1097–1102.
Bakke, J., Lie, Ø., Heegaard, E., Dokken, T., Haug, G.H., Birks, H.H., Dulski, P., Nilsen, T., 2009. Rapid oceanic and atmospheric changes during the Younger Dryas cold period. Nat. Geosci. 2, 202–205.
Berner, K.S., Koc, N., Godtliebsen, F., Divine, D., 2011. Holocene climate variability of the Norwegian Atlantic Current during high and low solar insolation forcing. Paleoceanography 26, PA2220. http://dx.doi.org/10.1029/2010PA002002.
Bethke, I., Li, C., Nisancioglu, K.H., 2012. Can we use ice sheet reconstructions to constrain meltwater for deglacial simulations? Paleoceanography 27, PA2205. http://dx.doi.org/10.1029/2011PA002258.
Birks, H.H., Aarnes, I., Bjune, A.E., Brooks, S.J., Bakke, J., Kühl, N., Birks, H.J.B., 2014. Late-glacial and early-Holocene climate variability reconstructed from multi-proxy records on Andøya, northern Norway. Quat. Sci. Rev. 89, 108–122.
Birks, H.H., Battarbee, R.W., Birks, H.J.B., 2000. The development of the aquatic ecosystem at Krakenes Lake, western Norway, during the late glacial and early Holocene – a synthesis. J. Paleolimnol. 23, 91–114.
Birks, H.H., Jones, V.J., Brooks, S.J., Birks, H.J.B., Telford, R.J., Juggins, S., Peglar, S.M., 2012. From cold to cool in northernmost Norway: Lateglacial and early Holocene multi-proxy environmental and climate reconstructions from Jansvatnet, Hammerfest. Quat. Sci. Rev. 33, 100–120.
Bjune, A.E., 2005. Holocene vegetation history and tree-line changes on a north – south transect crossing major climate gradients in sothern Norway – evidence from pollen and plant macrofossils in lake sediments. Rev. Palaeobot. Palynol. 123, 249–275.
Bjune, A.E., Bakke, J., Nesje, A., Birks, H.J.B., 2005. Holocene mean July temperature and winter precipitation in western Norway inferred from lake sediment proxies. Holocene 15.
Bjune, A.E., Birks, H.J.B., 2008. Holocene vegetation dynamics and inferred climate changes at Svanåvatnet, Mo i Rana, northern Norway. Boreas 37, 146–156.
Bjune, A.E., Birks, H.J.B., Peglar, S.M., Odland, A., 2010. Developing a modern pollen-climate calibration data set for Norway. Boreas 39, 674–688.
Bjune, A.E., Birks, H.J.B., Seppä, H., 2004. Holocene vegetation and climate history on a continental-oceanic transect in northern Fennoscandia based on pollen and plant macrofossils. Boreas 33, 211–223.
Blaauw, M., 2010. Methods and code for 'classical' age-modelling of radiocarbon sequences. Quat. Geochronol. 5, 512–518.

Blaga, C.I., Reichart, G.-J., Lotter, A.F., Anselmetti, F.S., Damsté, J.S.S., 2013. A TEX86 lake record suggests simultaneous shifts in temperature in Central Europe and Greenland during the last deglaciation. Geophys. Res. Lett. 40, 948–953.
Blaschek, M., Renssen, H., 2012. The Holocene thermal maximum in the Nordic Seas: the impact of Greenland Ice Sheet melt and other forcings in a coupled atmosphere-sea ice-ocean model. Clim. Past. 9, 1629–1643.
Blindheim, J., Borovkov, V., Hansen, B., Malmberg, S.A., Turrell, W.R., Østerhus, S., 2000. Upper layer cooling and freshening in the Norwegian Sea in relation to atmospheric forcing. Deep-Sea Res. 47, 655–680.
Bochkov, Y.A., 1982. Water temperature in the 0–200 m layer at the Kola Meridian in the Barents Sea, 1900–1981. Sb. Nauchnykh Tr. 46, 113–122. PINRO, Murmansk (in Russian).
Boitsov, V.D., Karsakov, A.L., Trofimov, A.G., 2012. Atlantic water temperature and climate in the Barents Sea, 2000–2009. ICES J. Mar. Sci. 69, 833–840.
Booth, B.B.B., Jones, C.D., Collins, M., Totterdell, I.J., Cox, P.M., Sitch, S., Huntingford, C., Betts, R.A., Harris, G.R., Lloyd, J., 2012. High sensitivity of future global warming to land carbon cycle processes. Environ. Res. Lett. 7, 024002. http://dx.doi.org/10.1088/021748-029326/024007/024002/024002.
Botev, Z.I., 2007. Kernel Density Estimation Using Matlab. Available at: http://www.mathworks.us/matlabcentral/fileexchange/authors/27236.
Botev, Z.I., Grotowski, J.F., Kroese, D.P., 2010. Kernel density estimation via diffusion. Ann. Stat. 38, 2916–2957.
Brauer, A., Haug, G.H., Dulski, P., Sigman, D.M., Negendank, J.F.W., 2008. An abrupt wind shift in western Europe at the onset of the Younger Dryas cold period. Nat. Geosci. 1, 520–523.
Bryden, H.L., Longworth, H.R., Cunningham, S.A., 2005. Slowing of the Atlantic meridional overturning circulation at 25°N. Nature 438, 655–657.
Byrkjedal, Ø., Kvamstø, N.G., Meland, M.Y., Jansen, E., 2006. Sensitivity of Last Glacial Maximum climate to sea ice conditions in the Nordic Seas. Clim. Dyn. 26, 473–487.
Cabedo-Sanz, P., Belt, S.T., Knies, J., Husum, K., 2012. Identification of contrasting seasonal sea ice conditions during the Younger Dryas. Quat. Sci. Rev..
Calvo, E., Grimalt, J., Jansen, E., 2002. High resolution U^{k}_{37} sea surface temperature reconstruction in the Norwegian Sea during the Holocene. Quat. Sci. Rev. 21, 1385–1394.
Carmack, E.C., 2007. The alpha/beta ocean distinction: a perspective on freshwater fluxes, convection, nutrients and productivity in high-latitude seas. Deep-Sea Res. Part II – Top. Stud. Oceanogr. 54, 2574–2598.
Cattiaux, J., Douville, H., Peings, Y., 2013. European temperatures in CMIP5: origins of present-day biases and future uncertainties. Clim. Dyn..
Cheng, J., Liu, Z., He, F., Otto-Bliesner, B.L., Colose, C., 2011. Impact of North Atlantic – GIN sea exchange on deglaciation evolution of the Atlantic meridional overturning circulation. Clim. Past. 7, 935–940.
Cheng, W., Chiang, J.C.H., Zhang, D., 2013. Atlantic meridional overturning circulation (AMOC) in CMIP5 models: RCP and historical simulations. J. Clim. 24, 7187–7197.
Chistyakova, N., Ivanova, E., Risebrobakken, B., Ovsepyan, E.A., Ovsepyan, Y.S., 2010. Reconstruction of Postglacial environments in the south – western Barents Sea based on foraminiferal assemblages. Oceanology 50, 573–581. http://dx.doi.org/10.1134/S0001437010040132 (English Translation).
CLIMAP, 1981. Seasonal Reconstructions of the Earth's Surface at the Last Glacial Maximum. In: Geological Society of America Map and Chart Series, vol. 38, p. 18.
Crocket, K.C., Vance, D., Gutjahr, M., Foster, G.L., Richards, D.A., 2011. Persistent Nordic deep-water overflow to the glacial North Atlantic. Geology 39, 515–518.
Cunningham, L.K., Austin, W.E.N., Knudsen, K.L., Eiríksson, J., Scourse, J.D., Wanamaker, A.D., Butler, P.G., Cage, A.G., Richter, T., Husum, K., Hald, M., Andersson, C., Zorita, E., Linderholm, H.W., Gunnarsson, B.E., Sicre, M.-A., Sejrup, H.P., Jiang, D., Wilson, R.J.S., 2013. Reconstruction of surface ocean conditions from the northeast Atlantic and Nordic seas during the last millennium. Holocene 23, 921–935.
Dahlgren, K.I.T., Vorren, T.O., 2003. Sedimentary environment and glacial history during the last 40 ka of the Voring continental margin, mid-Norway. Mar. Geol. 193, 93–127.
de Vernal, A., Hillaire-Marcel, C., Darby, D.A., 2005. Variability of sea ice cover in the Chukchi Sea (western Arctic Ocean) during the Holocene. Paleoceanography 20, PA4018. http://dx.doi.org/10.1029/2005PA001157.
de Vernal, A., Rosell-Melé, A., Kucera, M., Hillaire-Marcel, C., Eynaud, F., Weinelt, M., Dokken, T., Kageyama, M., 2006. Comparing proxies for the reconstruction of LGM sea-surface conditions in the northern North Atlantic. Quat. Sci. Rev. 25, 2820–2834.
Denton, G.H., Alley, R.B., Comer, G.C., Broecker, W.S., 2005. The role of seasonality in abrupt climate change. Quat. Sci. Rev. 24, 1159–1182.
Dokken, T.M., Jansen, E., 1999. Rapid changes in the mechanism of ocean convection during the last glacial period. Nature 401, 458–461.
Dong, B., Sutton, R.W., 2005. Mechanism if interdecadal thermohaline circulation variability in a coupled ocean-atmosphere GCM. J. Clim. 18, 1117–1135.
Duplessy, J.C., Shackleton, N.J., Fairbanks, R.G., Labeyrie, L., Oppo, D., Kallel, N., 1988. Deepwater source variations during the last climatic cycle and their impact on the global deepwater circulation. Paleoceanography 3, 343–360.
Ebbesen, H., Hald, M., 2004. Unstable younger dryas climate in the northeast North Atlantic. Geology 32, 673–676.
Eide, W., Birks, H.H., Bigelow, N.H., Peglar, S.M., Birks, H.J.B., 2006. Holocene forest development along the Setesdal valley, southern Norway, reconstructed from macrofossil and pollen evidence. Veg. Hist. Archaeobot. 15, 65–85.
Eiriksson, J., Bartels-Jonsdottir, H.B., Cage, A.G., Gudmundsdottir, E.R., Klitgaard-Kristensen, D., Marret, F., Rodrigues, T., Abrantes, F., Austin, W.E.N., Jiang, H., Knudsen, K.L., Sejrup, H.P., 2006. Variability of the North Atlantic Current during the last 2000 years based on shelf bottom water and sea surface temperatures along an open ocean/shallow marine transect in western Europe. Holocene 16, 1017–1029.
Eldevik, T., Nilsen, J.E.Ø., Iovino, D., Olsson, K.A., Sandø, A.B., Drange, H., 2009. Observed sources and variability of Nordic Seas overflow. Nat. Geosci. 2, 406–410.
Eldevik, T., Nilsen, J.E.Ø., 2013. The Arctic/Atlantic thermohaline circulation. J. Clim. 26, 8698–8705.
Fischer, N., Jungclaus, J.H., 2010. Effects of orbital forcing on atmosphere and ocean heat transports in Holocene and Eemian climate simulations with a comprehensive Earth system model. Clim. Past. 6, 155–168.
Førland, E.J., Benestad, R., Hanssen-Bauer, I., Haugen, E., Skaugen, T.E., 2011. Temperature and precipitation development at svalbard 1900–2100. Adv. Meteorol. 893790, doi:893710.891155/892011/893790.
Furevik, T., 2000. On anomalous sea surface temperatures in the Nordic Seas. J. Clim. 13, 1044–1053.
Furevik, T., Bentsen, M., Drange, H., Johannessen, J.A., Korablev, A., 2002. Temporal and spatial variability of the sea surface salinity in the Nordic Seas. J. Geophys. Res. 107 http://dx.doi.org/10.1029/2001JC001118.
Furevik, T., Bentsen, M., Drange, H., Kindem, I.K.T., Kvamstø, N.G., Sorteberg, A., 2003. Description and evaluation of the Bergen Climate Model: ARPEGE coupled with MICOM. Clim. Dyn. 21, 27–51.
Furevik, T., Nilsen, J.E.Ø., 2005. Large-scale atmospheric circulation variability and its impacts on the nordic seas ocean climate – a review. In: Drange, H., Dokken, T., Furevik, T., Gerdes, R., Berger, W. (Eds.), The Nordic Seas: an Integrated Perspective, AGU Geophysical Monograph, vol. 158, pp. 105–136.
Gladstone, R.M., Ross, I., Valdes, P.J., Abe-Ouchi, A., Braconnot, P., Brewer, S., Kageyama, M., Kitoh, A., Legrande, A., Marti, O., Ohgaito, R., Otto-Bliesner, B., Peltier, W.R., Vettoretti, G., 2005. Mid-Holocene NAO: a PMIP2 model intercomparison. Geophys. Res. Lett. 32, L16707. http://dx.doi.org/10.11029/12005GL023596.
Gregory, J.M., Dixon, K.W., Stouffer, R.J., Weaver, A.J., Driesschaert, E., Eby, M., Fichefet, T., Hasumi, H., Hu, A., Jungclaus, J.H., Kamenkovich, I.V., Levermann, A., Montoya, M., Murakami, S., Nawrath, S., Oka, A., Sokolev, A.P., Thorpe, R.B., 2005. A model intercomparison of changes in the Atlantic thermohaline circulation in response to increasing atmospheric CO_2 concentration. Geophys. Res. Lett. 32, L12703. http://dx.doi.org/10.11029/12005GL023209.
Gulev, S.K., Latif, M., Keenlyside, N., Park, W., Koltermann, K.P., 2013. North Atlantic Ocean control on surface heat flux on multidecadal timescales. Nature 499, 464–467.
Gyllencreutz, R., Mangerud, J., Svendsen, J.I., Lohne, Ø., 2007. DATED – a dating Database and GIS-based reconstruction of the Eurasian Deglaciation. Geol. Surv. Finl. Spec. Pap. 46, 113–120.
Hald, M., Salomonsen, G.R., Husum, K., Wilson, L.J., 2011. A 2000 year record of Atlantic Water temperature variability from the Malangen Fjord, northeastern North Atlantic. Holocene 21, 1049–1059.
Hall, I.R., Moran, S.B., Zahn, R., Knutz, P.C., Shen, C.-C., Edwards, R.L., 2006. Accelerated drawdown of meridional overturning in the late-glacial Atlantic triggered by transient pre-H event freshwater perturbation. Geophys. Res. Lett. 32, L16616. http://dx.doi.org/10.11029/12006GL026239.
Haney, R., 1971. Surface thermal boundary conditions for ocean circulation models. J. Phys. Oceanogr. 1, 241–428.
Hansen, B., Østerhus, S., 2000. North Atlantic-Nordic seas exchanges. Prog. Oceanogr. 45, 109–208.
Hansen, B., Turrell, W.R., Østerhus, S., 2001. Decreasing overflow from the Nordic seas into the Atlantic Ocean through the Faroe Bank channel since 1950. Nature 411, 928–930.
Hansen-Bauer, I., Tveito, O.E., Szewzyk-Bartnicka, H., 2006. Comparison of Grid-based and Station-based Regional Temperature and Precipitation Series. met.no report – climate.
Hátún, H., Sandø, A.B., Drange, H., Hansen, B., Valdimarsson, H., 2005. Influence of the Atlantic subpolar Gyre on the thermohaline circulation. Science 309, 1841–1844.
Helland-Hansen, B., Nansen, F., 1909. The Norwegian Sea – its physical oceanography based upon the Norwegian researchers 1900-1904. In: Hjort, J. (Ed.), Report on Norwegian Fishery and Marine Investigations, II. The Royal Department of Trade, Navigation and Industries.
Hemming, S.R., 2004. Heinrich event: massive late Pleistocene detritus layers of the North Atlantic and their global climate imprint. Rev. Geophys. 42, RG1005. http://dx.doi.org/10.1029/2003RG000128.
Holliday, N.P., Hughes, S.L., Bacon, S., Beszczynska-Möller, A., Hansen, A.W., Lavin, H., Loeng, H., Mork, K.A., Østerhus, S., Sherwin, T., Walczowski, W., 2008. Reversal of the 1960s to1990s freshening trend in the northeast North Atlantic and Nordic Seas. Geophys. Res. Lett. 35, L03614.
Hurrell, J.W., 1995. Decadal trends in the North Atlantic oscillation: regional temperatures and precipitation. Science 269, 676–679.
Isachsen, P.E., LaCasce, J.H., Pedlosky, J., 2007. Rossby wave instability and apparent phase speeds in large ocean basins. J. Phys. Oceanogr. 37, 1177–1191.
Isarin, R.F.B., Renssen, H., Vandenberghe, J., 1998. The impact of the North Atlantic Ocean on the Younger Dryas climate in northwestern and central Europe. J. Quat. Sci. 13, 447–453.

Jackob, D., Petersen, J., Eggert, B., Alias, A., Bøssing Christensen, O., Bouwer, L.M., Braun, A., Colette, A., Déqué, M., Georgievski, G., 2013. EURO-CORDEX: new high-resolution climate change projections for European impact research. Reg. Environ. Change.

Jennings, A.E., Knudsen, K.L., Hald, M., Hansen, C.V., Andrews, J.E., 2002. A mid-Holocene shift in Arctic sea-ice variability on the east Greenland Shelf. Holocene 12, 49–58.

Jennings, A.E., Weiner, N.J., 1996. Environmental changes in eastern Greenland during the last 1300 years: evidence from foraminifera and lithofacies in Nansen Fjord, 68°N. Holocene 6, 176–179.

Johns, T.C., Royer, J.F., Hoschel, I., Huebener, H., Roeckner, E., Manzini, E., May, W., Dufresne, J.L., Otterå, O.H., van Vuuren, D.P., Melia, D.S.Y., Giorgetta, M.A., Denvil, S., Yang, S., Fogli, P.G., Korper, J., Tjiputra, J.F., Stehfest, E., Hewitt, C.D., 2011. Climate change under aggressive mitigation: the ENSEMBLES multi-model experiment. Clim. Dyn. 37, 1975–2003.

Jones, P.D., Lister, D.H., Osborn, T.J., Harpham, C., Salmon, M., Morice, C.P., 2012. Hemispheric and large-scale land-surface air temperature variations: an extensive revision and an update to 2010. J. Geophys. Res. 117, D05127.

Kaufman, D.S., Ager, T.A., Anderson, N.J., Anderson, P.M., Andrews, J.T., Bartlein, P.J., Brubaker, L.B., Coats, L.L., Cwynar, L.C., Duvall, M.L., Dyke, A.S., Edwards, M.E., Eisner, W.R., Gajewski, K., Geirsdóttir, Á., Hu, F.S., Jennings, A.E., Kaplan, M.R., Kerwin, M.W., Lozhkin, A.V., MacDonald, G.M., Miller, G.H., Mock, C.J., Oswald, W.W., Otto-Bliesner, B.L., Porinchu, D.F., Rühland, K., Smol, J.P., Steig, E.J., Wolfe, B.B., 2004. Holocene thermal maximum in the western Arctic (0–180°W). Quat. Sci. Rev. 23, 529–560.

Kim, J.-H., Schneider, R.R., 2004. GHOST Global Database for Alkenone-derived Holocene Sea-surface Temperature Records. http://www.pangaea.de/Projects/GHOST/Holocene.

Kjennbakken, H., Sejrup, H.P., Haflidason, H., 2011. Mid- to late-Holocene oxygen isotopes from Voldafjorden, western Norway. Holocene 21, 897–909.

Klitgaard-Kristensen, D., Sejrup, H.P., Haflidason, H., 2001. The last 18 kyr fluctuations in Norwegian Sea surface conditions and implications for the magnitude of climatic change: evidence from the North Sea. Paleoceanorgaphy 16, 455–467.

Klitgaard-Kristensen, D., Sejrup, H.P., Haflidason, H., Berstad, I.M., 2004. Eight-hundred-year temperature variability from the Norwegian continental margin and the North Atlantic thermohaline circulation. Paleoceanography 19, PA2007. http://dx.doi.org/10.1029/2003PA000960.

Knorr, G., Lohmann, G., 2007. Rapid transitions in the Atlantic thermohaline circulation triggered by global warming and meltwater during the last deglaciation. Geochem. Geophys. Geosyst. 8, Q12006. http://dx.doi.org/10.11029/12007GC001604.

Knudsen, K.L., Jiang, H., Jansen, E., Eiríksson, J., Heinemeier, J., Seidenkrantz, M.-S., 2004. Environmental changes off North Iceland during the deglaciation and the Holocene: foraminifera, diatoms and stable isotopes. Mar. Micropaleontol. 50, 273–305.

Knudsen, M., 1900. Ein hydrographischer Lehrsatz. Annalen der Hydrographie und Maritimen Meteorlogie. Marit. Meteor 28, 316–320.

Koç Karpuz, N., Jansen, E., 1992. A high-resolution diatom record of the last deglaciation from the SE Norwegian Sea: documentation of rapid climatic changes. Paleoceanography 7, 499–520.

Koç, N., Klitgaard-Kristensen, D., Hasle, K., Forsberg, K.F., Solheim, A., 2002. Late glacial paleoceanography of Hinlopen Strait northern Svalbard. Polar Res. 21, 307–314.

Kucera, M., Rosell-Melé, A., Schneider, R.R., Waelbroeck, C., Weinelt, M., 2005a. Multiproxy approach for the reconstruction of the glacial ocean surface (MARGO). Quat. Sci. Rev. 24, 813–819.

Kucera, M., Weinelt, M., Kiefer, T., Pflaumann, U., Hayes, A., Weinelt, M., Chen, M., Mix, A., Barrows, T.T., Cortijo, E., Duprat, J., Juggins, S., Waelbroeck, C., 2005b. Reconstruction of sea-surface temperatures from assemblages of planktonic foraminifera: multi-technique approach based on geographically constrained calibration data sets and its application to glacial Atlantic and Pacific Oceans. Quat. Sci. Rev. 24, 951–998.

Kuhlbrodt, T., Griesel, A., Montoya, M., Levermann, A., Hofmann, M., Rahmstorf, S., 2007. On the driving processes of the Atlantic meridional ocerturning circulation. Rev. Geophys. 45, RG2001. http://dx.doi.org/10.1029/2004RG000166.

Latif, M., Park, W., Ding, H., Keenlyside, N.S., 2009. Internal and external North Atlantic Sector variability in the Kiel climate model. Meteorol. Z. 18, 433–443.

Leduc, G., Schneider, R., Kim, J.H., Lohmann, G., 2010. Holocene and Eemian sea surface temperature tends as revealed by alkenone and Mg/Ca paleothermometry. Quat. Sci. Rev. 29, 989–1004.

Lekens, W.A.H., Sejrup, H.P., Haflidason, H., Petersen, G.Ø., Hjelstuen, B., Knorr, G., 2006. Laminated sediments preceding Heinrich event 1 in the Northern North Sea and Southern Norwegian Sea: origin, processes and regional linkage. Mar. Geol. 216, 27–50.

Li, C., Battisti, D.S., Bitz, C.M., 2010. Can North Atlantic sea ice anomalies account for Dansgaard-Oeschger climate signals? J. Clim. 23, 5457–5475.

Liu, Z., Brady, E., Lynch-Stieglitz, J., 2003. Global ocean response to orbital forcing in the Holocene. Paleoceanography 18, 1041. http://dx.doi.org/10.1029/2002PA000819.

Liu, Z., Otto-Bliesner, B.L., He, F., Brady, E.C., Tomas, R., Clark, P.U., Carlson, A.E., Lynch-Stieglitz, J., Curry, W., Brook, E., Erickson, D., Jacob, R., Kutzbach, J., Cheng, J., 2009. Transient simulation of last deglaciation with a new mechanism for Bølling-Allerød warming. Science 325, 310–314.

Lohne, Ø.S., Mangerud, J., Birks, H.H., 2013. Precise 14C ages of the Vedde and Saksunarvat ashes and the Younger Dryas boundaries from western Norway and their comparison with the Greenland Ice Core (GICC05) chronology. J. Quat. Sci. 28, 490–500.

Mangerud, J., Bondevik, S., Gulliksen, S., Hufthammer, A.K., Høisæter, T., 2006. Marine ^{14}C reservoir ages for 19th century whales and molluscs from the Northe Atlantic. Quat. Sci. Rev. 25, 3228–3245.

Mangerud, J., Gyllencreutz, R., Lohne, Ø., Svendsen, J.I., 2011. Glacial history in Norway. In: Ehlers, J., Gibbard, P.L., Hughes, P.D. (Eds.), Developments in Quarternary Science. Elsevier, Amsterdam, The Netherlands, pp. 279–298.

Marchal, O., Cacho, I., Stocker, T.F., Grimalt, J.O., Calvo, E., Martrat, B., Shackleton, N.J., Vautravers, M., Cortijo, E., van Kreveld, S., Andersson, C., Koç, N., Chapman, M., Sbaffi, L., Duplessy, J.C., Sarnthein, M., Turon, J.L., Duprat, J., Jansen, E., 2002. Apparent long-term cooling of the sea surface in the northeast Atlantic and Mediterranean during the Holocene. Quat. Sci. Rev. 21, 455–483.

Marcott, S.A., Clark, P.U., Padman, L., Klinkhammer, G.P., Springer, S.R., Liu, Z., Otto-Bliesner, B.L., Carlson, A.E., Ungerer, A., Padman, J., He, F., J., C., Schmittner, A., 2011. Ice-shelf collapse from subsurfcae warming as a trigger for Heinrich events. PNAS 108, 13415–13419.

Marcott, S.A., Shakun, J.D., Clark, P.U., Mix, A.C., 2013. A reconstruction of regional and global temperature for the past 11,300 years. Science 339, 1198–1201.

MARGO Project members, 2009. Constraints on the magnitude and patterns of ocean cooling at the Last Glacial Maximum. Nat. Geosci. 2, 127–132.

Marshall, J., Kushnir, Y., Battisti, D., Chang, P., Czaja, A., Dickson, R.R., Hurrell, J., McCartney, M., Saravanan, R., Visbeck, M., 2001. North Atlantic Climate Variability: phenomena, impacts and mechanisms. Int. J. Climatol. 21, 1863–1898.

Marshall, J., Schott, F., 1999. Open-ocean convection: observations, theory, and models. Rev. Geophys. 37, 1–64.

Martrat, B., Grimalt, J.O., Villanueva, J., van Kreveld, S., Sarnthein, M., 2003. Climatic dependence of the organic matter contributions in the north eastern Norwegian Sea over the last 15,000 years. Org. Geochem. 34, 1057–1070.

Mauritzen, C., 1996a. Production of dense overflow waters feeding the North Atlantic across the Greenland-Scotland Ridge. 2. An inverse model. Deep Sea Res. 43, 807–835.

Mauritzen, C., 1996b. Production of dense overflow waters feeding the North Atlantic across the Greenland-Scotland Ridge. Part 1: evidence for a revised circulation scheme. Deep Sea Res. 43, 769–837.

McManus, J.F., Francois, R., Gherardi, J.-M., Keigwin, l.D., Brown-Leger, S., 2004. Collapse and rapid resumption of Atlantic meridional circulation linked to deglacial climate changes. Nature 428, 834–837.

Meehl, G.A., Stocker, T.F., Collins, W.D., Friedlingstein, P., Gaye, A.T., Gregory, J.M., Kitoh, A., Knutti, R., Mutphy, J.M., Noda, A., Raper, S.C.B., Watterson, I.G., Weaver, A.J., Zhao, Z.-C., 2007. Global climate projections. In: Solomon, S., Qin, D., Manning, M., Chen, Z., Marquis, M., Averyt, K.B., Tignor, M., Miller, H.L. (Eds.), Climate Change 2007: the Physical Science Basis. Contribution of Working Group I to the Fourth Assessment Report of the Intergovernmental Panel on Climate Change. Cambridge University Press, Cambridge, UK and New York, USA.

Meland, M.Y., Dokken, T.M., Jansen, E., Hevrøy, K., 2008. Water mass properties and exchange between the Nordic seas and the northern North Atlantic during the period 23–6 ka: benthic oxygen isotope evidence. Paleoceanography 23, PA1210. http://dx.doi.org/10.1029/2007PA001416.

Meland, M.Y., Jansen, E., Elderfield, H., 2005. Constraints on SST estimates for the northern North Atlantic/Nordic Seas during the LGM. Quat. Sci. Rev. 24, 835–852.

Miller, G.H., Geirsdottir, A., Zhong, Y.F., Larsen, D.J., Otto-Bliesner, B.L., Holland, M.M., Bailey, D.A., Refsnider, K.A., Lehman, S.J., Southon, J.R., Anderson, C., Bjornsson, H., Thordarson, T., 2012. Abrupt onset of the Little Ice Age triggered by vulcanism and sustained by sea-ice/ocean feedbacks. Geophys. Res. Lett. 39, L02708. http://dx.doi.org/10.01029/02011GL050168.

Morice, C.P., Kennedy, J.J., Rayner, N.A., Jones, P.D., 2012. Quantifying uncertainties in global and regional temperature change using an ensemble of observational estimates: the HadCRUT4 data set. J. Geophys. Res. 117, D08101.

Mork, K.A., Blindheim, J., 2000. Variations in the Atlantic inflow to the Nordic Seas, 1955–1996. Deep-Sea Res. 47, 1035–1057.

Moros, M., Emeis, K., Risebrobakken, B., Snowball, I., Kuijpers, A., McManus, J., Jansen, E., 2004. Sea surface temperatures and ice rafting in the Holocene North Atlantic: climate influences on northern Europe and Greenland. Quat. Sci. Rev. 23, 2113–2126.

Müller, J., Masse, G., Stein, R., Belt, S.T., 2009. Variability of sea-ice conditions in the Fram Strait over the past 30,000 years. Nat. Geosci. 2, 772–776.

Müller, J., Werner, K., Stein, R., Fahl, K., Moros, M., Jansen, E., 2012. Holocene cooling culminates in sea ice oscillations in Fram Strait. Quat. Sci. Rev. 47, 1–14.

Murton, J.B., Bateman, M.D., Dallimore, S.R., Teller, J.T., Yang, Z., 2010. Identification of Younger Dryas outburst flood path from Lake Agassiz to the Arctic Ocean. Nature 464, 740–743.

Nansen, F., 1906. Northern Waters:Captain Roald Amundsen's Oceanographic Observations in the Arctic Seas in 1901 with a Discussion of the Origin of the Bottomwaters of the Nortnern Seas. Videnskabs-Selskabets Skr. 1. Matematisk-Naturv. Klasse 1, Fridtjof Nansens fond, Dybvad. Christiania, pp. 1–145.

Nesje, A., Dahl, S.O., Thun, T., Nordli, Ø., 2008. The 'Little Ice Age' glacial expansion in western Scandinavia: summer temperature or winter precipitation? Clim. Dyn. 30, 789–801.

Nesje, A., Jansen, E., Birks, J.B., Bjune, A.E., Bakke, J., Andersson Dahl, C., Dahl, S.O., Klitgaard-Kristensen, D., Lauritzen, S.E., Lie, Ø., Løvlie, R., Risebrobakken, B., Svendsen, J.I., 2005. Holocene climate variability in the North Atlantic region: a

review of marine and terrestrial evidence. In: Drange, H., Dokken, T., Furevik, T., Gerdes, R., Berger, W.H. (Eds.), The Nordic Seas, an Integrated Perspective, AGU Geophysical Monograph, pp. 289–322.
Nilsen, J.E.Ø., Falck, E., 2006. Variations of mixed layer properties in the Norwegian Sea for the period 1948–1999. Prog. Oceanogr. 70, 58–90.
Nilsen, J.E.Ø., Hátún, H., Mork, K.A., Valdimarsson, H., 2008. The NISE Dataset. Technical Report 08-01. Faeroese Fisheries Laboratory, Box 3051, Tórshavn, Faroe Islands.
Nøst, O.A., Isachsen, P.E., 2003. The large-scale time-mean ocean circulation in the Nordic Seas and Arctic Ocean estimated from simplified dynamics. J. Mar. Sci. 61, 175–210.
Olsen, J., Anderson, N.J., Knudsen, M.F., 2012. Variability of the North Atlantic Oscillation over the past 5200 years. Nat. Geosci. 5, 808–812.
Olsen, S.M., Hansen, B., Quadfasel, D., Østerhus, S., 2008. Observed and modelled stability of overflow across the Greenland-Scotland ridge. Nature 455, 519–522.
Oppo, D.W., Lehman, S.J., 1993. Mid-depth circulation of the subpolar North-Atlantic during the Last Glacial Maximum. Science 259, 1148–1152.
Orvik, K.A., Niiler, P., 2002. Major pathways of Atlantic water in the northern North Atlantic and Nordic Seas towards Arctic. Geophys. Res. Lett. 29, 1896.
Orvik, K.A., Skagseth, Ø., 2003. The impact of the wind stress curl in the North Atlantic on the Atlantic inflow to the Norwegian Sea toward the Arctic. Geophys. Res. Lett. 30, 1884.
Orvik, K.A., Skagseth, Ø., 2005. Heat flux variations in the eastern Norwegian Atlantic Current toward the Arctic from moored instruments, 1995–2005. Geophys. Res. Lett. 32, L14610.
Østerhus, S., Turrell, W., Jónsson, S., Hansen, B., 2005. Measured volume, heat, and salt fluxes from the Atlantic to the Arctic Mediterranean. Geophys. Res. Lett. 32, L07603. http://dx.doi.org/10.01029/02004GL022188.
Otterå, O.H., Bentsen, M., Bethke, I., Kvamstø, N.G., 2009. Simulated pre-industrial climate in Bergen Climate Model (version 2):model description and large-scale circulation features. Geosci. Model Dev. 2, 197–212.
Otterå, O.H., Bentsen, M., Drange, H., Sou, L., 2010. External forcing as a metronome for Atlantic multidecadal variability. Nat. Geosci. 3, 688–694.
Otto-Bliesner, B.L., Hewitt, C.D., Marchitto, T.M., Brady, E., Abe-Ouchi, A., Crucifix, M., Murakami, S., Weber, S.L., 2007. Last Glacial Maximum ocean thermohaline circulation: PMIP2 model intercomparison and data constraints. Geophys. Res. Lett. 34, L12706. http://dx.doi.org/10.11029/12007GL029475.
Overland, J.E., Wood, K.R., Wang, M., 2011. Warm Arctic-cold continents: Impacts of the newly open Arctic Sea. Polar Res. 30, 15787.
Pausata, F.S.R., Li, C., Wettstein, J.J., Nisancioglu, K.H., Battisti, D.S., 2009. Changes in atmospheric variability in a glacial climate and the impacts on proxy data: a model intercomparison. Clim. Past. 5, 489–502.
Polyakov, I.V., Alekseev, G.V., Bekryaev, R.V., Bhatt, U., Colony, R.L., Johnson, M.A., Karklin, V.P., Makshtas, A.P., walsh, D., Yulin, A.V., 2002. Observationally based assessment of polar amplification of global warming. Geophys. Res. Lett. 29, 1878.
Polyakov, I.V., Beszczynska, A., Carmack, E.C., Dmitrenko, I.A., Farbach, E., Frolov, I.E., Gerdes, R., Hansen, E., Holfort, J., V., I.V., Johnson, M.A., Karcher, M., Kauker, F., Morison, J., Orvik, K.A., Schauer, U., Simmons, H.L., Skagseth, Ø., Sokolov, V.T., Steele, M., Timokhov, L.A., Walsh, D., Walsh, J.E., 2005. One more step toward a warmer Arctic. Geophys. Res. Lett. 32, L17605. http://dx.doi.org/10.11029/12005GL023740.
Prentice, R.L., 1980. Analysis of multivariate failure time data with competing risks. Biometrics 36, 190.
Rahmstorf, S., 2002. Ocean circulation and climate during the past 120,000 years. Nature 419, 207–214.
Rasmussen, S.O., Andersen, K.K., Svensson, A.M., Steffensen, J.P., Vinther, B.M., Clausen, H.B., Siggard-Andersen, M.-L., Johnsen, S.J., Larsen, L.B., Dahl-Jensen, D., Bigler, M., Röthlisberger, R., Fischer, H., Goto-Azuma, K., Hansson, M.E., Ruth, U., 2006. A new Greenland ice core chronology for the last glacial termination. J. Geophys. Res. 111, D06102. http://dx.doi.org/10.01029/02005JD006079.
Rasmussen, S.O., Bigler, M., Blockley, S.P.E., Blunier, T., Buchardt, S.L., Clausen, H.B., Cvijanovic, I., Dahl-Jensen, D., Johnsen, S.J., Fischer, H., Gkins, V., Guillevic, M., Hoek, W.Z., Lowe, I.J., Pedro, J., Topp, T., Seierstad, I.K., Steffensen, J.P., Svensson, A.M., Vallelonga, P., Vinther, B.M., Walker, M.J.C., Wheatley, J.J., Winstrup, M., 2014. A stratigraphic framework for robust naming and correlation of abrupt climatic changes during the last glacial period based on three synchronized Greenland ice core records (submitted for publication). Quat. Sci. Rev..
Rasmussen, T.L., Thomsen, E., 2008. Warm Atlantic surface water inflow to the Nordic Seas 34–10 calibrated ka B.P. Paleoceanography 23, PA1201. http://dx.doi.org/10.1029/2007PA001453.
Rasmussen, T.L., Thomsen, E., Slubowska, M.A., Jessen, S., Solheim, A., Koç, N., 2007. Paleoceanographic evolution of the SW Svalbard margin (76N) since 20,000 ^{14}C yr BP. Quat. Res. 67, 100–114.
Raymo, M.E., Oppo, D.W., Flower, B.P., Hodell, D.A., McManus, J.F., Venz, K.A., Kleiven, H.F., McIntyre, K., 2004. Stability of North Atlantic water masses in face of pronounced climate variability during the Pleistocene. Paleoceanography 19, PA2008. http://dx.doi.org/10.1029/2003PA000921.
Reimer, P.J., Bard, E., Bayliss, A., Beck, J.W., Blackwell, P.G., Bronk Ramsey, C., Buck, C.E., Cheng, H., Edwards, R.L., Friedrich, M., Grootes, P.M., Guilderson, T.P., Haflidason, H., Hajdas, I., Hatté, C., Heaton, T.J., Hoffmann, D.L., Hogg, A.G., Hughen, K.A., Kaiser, K.F., Kromer, B., Manning, S.W., Niu, M., Reimer, R.W., Richards, D.A., Scott, E.M., Southon, J.R., Staff, R.A., Turney, C.S.M., van der Plicht, J., 2013. Intcal13 and Marine13 radiocarbon age calibration curves 0–50,000 years cal BP. Radiocarbon 55, 1869–1887.
Renssen, H., Goosse, H., Muscheler, R., 2006. Coupled climate model simulation of Holocene cooling events: oceanic feedback amplifies solar forcing. Clim. Past 2, 79–90.
Rhines, P., Häkkinen, S., Josey, S., 2008. Is oceanic heat transport significant in the climate system? In: Dickson, B., Meincke, J., Rhines, P. (Eds.), Arctic – Subarctic Ocean Fluxes: Defining the Role of the Northern Seas in Climate, pp. 87–109.
Richter, K., Maus, S., 2011. Interannual variability in the hydrography of the Norwegian Atlantic Current: frontal versus advective response to atmospheric forcing. J. Geophys. Res. – Ocean. 116, C12031. http://dx.doi.org/10.1029/12011JC007311.
Richter, K., Segtnan, O.H., Furevik, T., 2012. Variability of the Atlantic inflow to the Nordic Seas and its cause inferred from observations of sea surface hight. J. Geophys. Res. – Oceans 117, C04004. http://dx.doi.org/10.1029/2011JC007719.
Risebrobakken, B., Dokken, T., Smedsrud, L.H., Andersson, C., Jansen, E., Moros, M., Ivanova, E.V., 2011. Early Holocene temperature variability in the Nordic Seas: the role of oceanic heat advection versus changes in orbital forcing. Paleoceanography 26, PA4206. http://dx.doi.org/10.1029/2011PA002117.
Risebrobakken, B., Jansen, E., Andersson, C., Mjelde, E., Hevrøy, K., 2003. A high-resolution study of Holocene paleoclimatic and paleoceanographic changes in the Nordic Seas. Paleoceanography 18, 1017. http://dx.doi.org/10.1029/2002PA000764.
Risebrobakken, B., Moros, M., Ivanova, E., Chistyakova, N., Rosenberg, R., 2010. Climate and oceanographic variability in the SW Barents Sea during the Holocene. Holocene 20, 609–621.
Rørvik, K.-L., Laberg, J.S., Hald, M., Ravna, E.K., Vorren, T.O., 2010. Behaviour of the northwestern part of the Fennoscandian Ice Sheet during the Last Glacial Maximum – a response to external forcing. Quat. Sci. Rev. 29, 2224–2237.
Rudels, B., 2010. Constraints on exchanges in the Arctic Mediterranean – do they exist and can they be of use? Tellus Ser. – Dyn. Meteorol. Oceanogr. 62, 109–122.
Saloranta, T.M., Haugan, P.M., 2004. Northward cooling and freshening of the warm core of the West Spitsbergen Current. Polar Res. 23, 79–88.
Schmittner, A., Latif, M., Schneider, B., 2005. Model projections of the North Atlantic thermohaline circulation for the 21st century assessed by observations. Geophys. Res. Lett. 32, L23710.
Seppä, H., 1996. Post-glacial dynamics of vegetation and tree-lines in the north of Fennoscandia. Fennia 174, 1–96.
Seppä, H., 1998. Postglacial trends in palynological richness in the northern Fennoscandian tree-line area and their ecological interpretation. Holocene 8, 43–53.
Seppä, H., Birks, H.H., Birks, H.J.B., 2002. Rapid climatic changes during the Greenland stadial 1 (Younger Dryas) to early holocene transition on the Norwegian Barents Sea coast. Boreas 31, 215–225.
Seppä, H., Birks, H.J.B., 2001. July mean temperature and annual precipitation trends during the Holocene in the Fennoscandian tree-line area: pollen-based reconstructions. Holocene 11, 527–539.
Seppä, H., Bjune, A.E., Telford, R.J., Birks, H.J.B., Veski, S., 2009. Last nine-thousand years of temperature variability in Northern Europe. Clim. Past. 5, 523–535.
Serreze, M.C., Barry, R.G., 2011. Processes and impacts of Arctic amplification: a research synthesis. Global Planet. Change 77, 85–96.
Serreze, M.C., Holland, M.M., Stroeve, J., 2007. Perspectives on the Arctic's rapidly shrinking sea-ice cover. Science 315, 1533–1536.
Shakun, J.D., Clark, P.U., He, F., Marcott, S.A., Mix, A.C., Liu, Z., Otto-Bliesner, B., Schmittner, A., Bard, E., 2012. Global warming preceded by increasing carbon dioxide concentrations during the last deglaciation. Nature 484, 49–54.
Skagseth, Ø., Furevik, T., Ingvaldsen, R., Loeng, H., Mork, K.A., Orvik, K.A., Ozhigin, V., 2008. Volume and heat transports to the arctic ocean via the norwegian and barents sea. In: Dickson, R.R., Meincke, J., Rhines, P. (Eds.), Arctic-subarctic Ocean Fluxes. Springer, Dortrecht, pp. 45–64.
Skagseth, Ø., Orvik, K.A., Furevik, T., 2004. Coherent variability of the Norwegian Atlantic Slope Current derived from TOPEX/ERS altimeter data. Geophys. Res. Lett. 31, L14304. http://dx.doi.org/10.11029/12004GL020057.
Slubowska, M.A., Koç, N., Rasmussen, T.L., Klitgaard-Kristensen, D., 2005. Changes in the flow of Atlantic water into the Arctic Ocean since the last deglaciation: evidence from the northern Svalbard continental margin, 80°N. Paleoceanography 20, PA4014. http://dx.doi.org/10.1029/2005PA001141.
Slubowska-Woldengen, M., Koç, N., Rasmussen, T.L., Klitgaard-Kristensen, D., Hald, M., Jennings, A.E., 2008. Time-slice reconstructions of ocean circulation changes on the continental shelf in the Nordic and Barents Seas during the last 16,000 cal yr B.P. Quat. Sci. Rev. 27, 1476–1492.
Slubowska-Woldengen, M., Rasmussen, T.L., Koç, N., Klitgaard-Kristensen, D., Nilsen, F., Solheim, A., 2007. Advection of Atlantic Water to the western and northern Svalbard shelf since 17,500 cal yr BP. Quat. Sci. Rev. 26, 463–478.
Spall, M.A., Pickart, R.S., 2001. Where does dense water sink? A subpolar gyre example. J. Phys. Oceanogr. 31, 810–825.
Spielhagen, R.F., Werner, K., Aagaard-Sørensen, S., Zamelczyk, K., Kandiano, E.S., Budeus, G., Husum, K., Marchitto, T.M., Hald, M., 2011. Enhanced modern heat Transfer to the arctic by warm Atlantic water. Science 331, 450–453.
Stanford, J.D., Rohling, E.J., Bacon, S., Roberts, A.P., Grousset, F.E., Bolshaw, M., 2011. A new concepth for the paleoceanographic evolution of Heinrich event 1 in the North Atlantic. Quat. Sci. Rev. 30, 1047–1066.

Stanford, J.D., Rohling, E.J., Hunter, S.E., Roberts, A.P., Rasmussen, S.O., Bard, E., McManus, J., Fairbanks, R.G., 2006. Timing of meltwater pulse 1a and climate responses to meltwater injections. Paleoceanography 21, PA4103. http://dx.doi.org/10.1029/2006PA001340.

Stenchikov, G., Delworth, T.L., Ramaswamy, V., Stouffer, R.J., Wittenberg, A., Zeng, F.R., 2009. Vulcanic signals in oceans. J. Geophys. Res. – Atmos., D16104. http://dx.doi.org/10.11029/12008JD011673.

Stephenson, D.B., Pavan, V., Collins, M., Junge, M.M., Quadrelli, R., 2006. North Atlantic Oscillation response to transient greenhouse gas forcing and the impact on European winter climate: a CMIP2 multi-model assessment. Clim. Dyn. 27, 401–420.

Stigebrandt, A., 1985. On the hydrographic and ice conditions in the northern North Atlantic during different phases of a glaciation cycle. Paleogeogr. Paleoclimatol. Paleoecol. 50, 303–321.

Straneo, F., 2006. On the connection between dense water formation, overturning and poleward heat transport in a convective basin. J. Phys. Oceanogr. 36, 1822–1840.

Stroeve, J.C., Serreze, M., Holland, M., Kay, J.E., Maslanik, J.A., Barrett, A.P., 2012. The Arctic's rapidly shrinking sea ice cover: a research synthesis. Clim. Change 110, 1005–1027.

Swingedouw, D., Terray, L., Cassou, C., Voldoire, A., Salas-Mélia, D., Servonnat, J., 2011. Natural forcing of climate during the last millennium: fingerprint of solar variability. Clim. Dyn. 36, 1349–1364.

Tarasov, L., Peltier, W.R., 2005. Arctic freshwater forcing of the Younger Dryas cold reversal. Nature 435, 662–665.

ter Braak, C.J.F., Juggins, S., 1993. Weighted averaging partial least squares regression (WA-PLS): an improved method for reconstructing environmental variables from species assemblages. Hydrobiologia 269/270, 485–502.

ter Braak, C.J.F., Prentice, I.C., 1988. A theory of gradient analysis. Adv. Ecol. Res. 18, 271–317.

ter Braak, C.J.F., van Dam, H., 1989. Inferring pH from diatoms: a comparison of old and new calibration methods. Hydrobiologia 178, 209–223.

Weaver, A.J., Sedlacek, J., Eby, M., Alexander, K., Crespin, E., Fichefet, T., Philippon-Berthier, G., Joos, F., Kawamlya, M., Matsumoto, K., Steinacher, M., Tachiliri, K., Tokos, K., Yoshimori, M., Zickfeld, K., 2012. Stability of the Atlantic meridional overturning circulation: a model intercomparison. Geophys. Res. Lett. 39, L20709. http://dx.doi.org/10.21029/22012GL053763.

Worthington, L.V., 1970. Norwegian Sea as a Mediterranean basin. Deep-Sea Res. 17, 77–84.

Wunsch, C., 2006. Abrupt climate change: an alternative view. Quat. Res. 65, 191–203.

Zanchettin, D., Timmreck, C., Graf, H.-F., Rubino, A., Lorentz, S., Lohmann, G., Krüger, K., Jungclaus, J.H., 2012. Bi-decadal variability excited in the coupled ocean-atmosphere system by strong tropical vulcanic eruptions. Clim. Dyn. 39, 419–444.